2018

LCD 3D Printing of a Photocurable Elastomer for Tissue Engineering

Beatriz Luiza De Souza
South Dakota State University

LCD 3D PRINTING OF A PHOTOCURABLE ELASTOMER FOR TISSUE ENGINEERING

BY

BEATRIZ LUIZA DE SOUZA

A thesis submitted in partial fulfillment of the requirements for the

Master of Science

Major in Mechanical Engineering

South Dakota State University

2018

LCD 3D PRINTING OF A PHOTOCURABLE ELASTOMER FOR TISSUE ENGINEERING

BEATRIZ LUIZA DE SOUZA

This thesis is approved as a creditable and independent investigation by a candidate for the Master of Science in Mechanical Engineering degree and is acceptable for meeting the thesis requirements for this degree. Acceptance of this does not imply that the conclusions reached by the candidate are necessarily the conclusions of the major department.

Todd Letcher, Ph.D.
Thesis Advisor Date

Kurt Basset, Ph.D.
Head, Department of Mechanical Engineering Date

Dean, Graduate School Date

ACKNOWLEDGEMENTS

I would like to take this opportunity to express my sincere appreciation to my advisor Dr. Todd Letcher for his understanding, support, tolerance, inspiration and confidence in my abilities. The combination of his background and insight guided me through the completion of my undergraduate and master's work. I cannot express how grateful I am for his excellent guidance. I would also like to thank Dr. Fereidoon Delfanian for financially supporting me through South Dakota State University's METLAB, and for allowing me to use this unique facility. I would like to thank the Mechanical Engineering department for the financial support to my project. I would also like to thank Dr. Anamika Prasad for providing needed advice and assistance in this project and Paul Melino for his assistance with the 3D printer.

I am grateful to the tremendous efforts of Dr. Mark Messerli and Dr. Cheng Zhang, in doing numerous experiments. They helped me navigate my project on a biological and chemistry approach respectively for this multidisciplinary project. I am thankful to Dr. Stephen Gent, Dr. Chamika Hawkings-Taylor and Dr. Anamika Prasad for being my committee members, and Dr. Abdulsalam Alqahtani for allowing me to use his laboratory for FTIR experiments.

I thank all my friends at home and abroad for their friendship and support during my master's degree. They have been providing me a pleasant social atmosphere and emotional support. I especially appreciate the love and reassurance from my boyfriend Eric Heidel. Finally, I wish to express my infinite gratitude to my parents and other members in my family.

CONTENTS

LIST OF SYMBOLS AND ABBREVIATIONS

3D	Three - Dimensional
C	Celsius
CHO	Chinese Hamster Ovary
DA	Degree of Acrylation
DI	Deionized
DMAP	2,2-dimethoxy2-phenylacetophenone
DMD	Digital Mirror Device
DNA	Deoxyribonucleic acid
DSC	Differential Scanning Calorimetry
FDM	Fusion Deposition Modeling
FFF	Free Form Fabrication
FTIR	Fourier-Transform Infrared Spectroscopy
G′	Storage Modulus
G″	Loss Modulus
HA	Hyaluronic Acid
Hz	Hertz
LaBP	Laser Assisted Bioprinting
LAP	Lithium Phenyl-2,4,6-trimethylbenzoylphosphinate
LCD	Liquid-Crystal Display
MPa	Mega Pascals Unit
P4HB	Prolyl 4-hydroxylase Subunit Beta
PBS	Phosphate Buffered Saline

PCL	Polycaprolactone
PGA	Polyglycolic Acid
PGS	Polyglycerol Sebacate
PGSA	Polyglycerol Sebacate Acrylate
PHB	Poly(3-hydroxybutyrate)
PLA	Poly (Lactic Acid)
PLGA	Poly-dl-lactic-co-glycolic Acid
SLA	Stereolithography
TEA	Triethylamine
UV	Ultra Violet
VA086	2,2'-Azobis[2-methyl-N-(2-hydroxyethyl) propionamide]

LIST OF FIGURES

LIST OF TABLES

ABSTRACT

LCD 3D PRINTING OF A PHOTOCURABLE ELASTOMER FOR TISSUE ENGINEERING

BEATRIZ LUIZA DE SOUZA

2018

Three-dimensional scaffolding is an emerging research area in biomedical and tissue engineering. Scaffolds provide the possibility of growing tissues in a controlled environment, with desired characteristics and properties towards a specific application. A new method to 3D print biodegradable and biocompatible material called Polyglycerol Sebacate Acrylate (PGSA) is demonstrated. PGSA is essentially an acrylated form of PGS using photoinitiator to become a photocurable resin suitable for liquid crystal display (LCD) 3D printing. PGSA was selected because its rheological and crosslinking behavior (and hence its mechanical properties) can be controlled by changes in curing time, temperature, and pressure. This material has been proven cytocompatible, and capable of replicating tissue shapes according to detailed computer-aided designs.

A modified LCD 3D printer consisting of a vat of photocurable resin that is suspended above an LCD screen was used. Using a UV-LED light source, the object is built layer-by-layer until the model is completed. It differs from traditional 3D printing in that the whole layer is cured simultaneously, making this a much faster process. The resin needs to be not only be photocurable, but also have optimal rheological property for control of 3D printing parameters. Here, we developed a modified PGSA suitable for LCD 3D printing. The material viscosity was characterized using a rheometer. Additionally, the material was characterized using Fourier Transform Infrared Spectroscopy (FTIR) Nicolet

380. Tensile tests were conducted on the build sample to determine its mechanical properties. Last, biocompatibility tests were performed on the cell-seeded scaffold to validate its cell adhesion, cell proliferation, and cell viability.

LCD 3D printing is simple, fast and can provide excellent resolution due to small pixel sizes of the LCD screen. Therefore, combining LCD 3D printing and PGSA is a very promising tool for biomedical applications by allowing complex biocompatible, elastomeric tissue scaffolds that can be highly customized without modifying the manufacturing process.

1 INTRODUCTION

Over the last two decades, 3D printing has revolutionized health care, with the possibility of tissue and organ fabrication, anatomical models, customized prosthetics, and drug delivery applications [1]. In tissue engineering, the creation of scaffolds for tissue replacements is critical due to high demand of surgical repairs, resulting from athletic injuries, aging, and diseases [2]. An effective scaffold needs to be of suitable mechanical strength, biocompatible, and should allow surfaces for cell growth, cell adherence, and cell proliferation [2]. Moreover, the geometry and the porosity of the scaffold should be optimally structured to guide the cells and promote diffusion of nutrients and waste [3]. Finally, depending on the application, the scaffold may also need to degrade in a controlled matter, without producing toxic products, and with minimal inflammatory response.

The architecture of the scaffold is of extreme importance. Interconnected pore structures, porous size and high porosity are essential to guarantee cell penetration, satisfactory diffusion of nutrients and waste products, and for the scaffold to successfully replicate an extra-cellular matrix [4]. The pore interconnectivity is important for cell ingrowth, vascularization, and nutrient diffusion for cell survival [5]. Pore size is critical for an optimum scaffold design. The cells connect with the scaffold via ligands (chemical groups) on the material. The pores must be large enough to allow the cells to migrate into the structure, where they can bound with the scaffold, but small enough to create an appropriately high specific surface, and assist with proliferation [6].

In general, the pore size needs to be inside a range close to the size of the cells desired for the target tissue replacement, since either too small or too large pore sizes will make it harder for cells to adhere and proliferate in the scaffold [7]. Therefore, the optimum pore size for specific cell types was found by previous experiments - 5 μm for neovascularization, 5–15 μm for fibroblast ingrowth, 20–125 μm for regeneration of adult mammalian skin, 100–350 μm for regeneration of bone, 40–100 μm for osteoid ingrowth, and 20 μm for the ingrowth of hepatocytes [8].

Additionally, the balance between porosity and the mechanical properties of the scaffold is critical for a successful scaffold on tissue engineering. While high porosity and pore sizes ease diffusion of nutrients and oxygen and enhance cell ingrowth, it also decreases the mechanical properties of the scaffold due to high voids in the volume [9]. Thus, the stiffness of the scaffold decreases as porosity increases [10]. For an optimum scaffold design, the equilibrium between these two properties is essential to keep enough mechanical strength to preserve the scaffold integrity until new tissue is formed.

Traditional methods of fabricating scaffolds using polymer materials includes molding [11], solvent casting and particulate leaching [12], gas foaming [13], and electrospinning [14]. Each of these traditional fabrication methods provide certain limitations on scaffold structure in terms of its geometry and porosity, and requires great fabrication skills to maintain consistency in the reproducibility of the scaffold [2, 6]. Additive manufacturing (also known as three-dimensional (3D) printing or rapid prototyping) allows much higher control on macroscale and microscale of the scaffold dimensions and architectures, with better design repeatability, being a more reliable and improved manufacturing process for tissue engineering scaffolds [15]. In additive

manufacturing, objects are created by adding material, layer by layer. The layers are generated through extrusion deposition, solidification, photopolymerization, or binding [3]. A model to be printed is first generated in a computer-aided design (CAD) program and imported into a 3D printing software, which translates the data into parameters and codes for the 3D printer.

The most common 3D printing technique is Fused Deposition Modeling (FDM) which is a material extrusion based method. It is commonly used for biomedical applications, mostly with syringe type of extruder with hydrogels [15-18]. However, hydrogels are not easy to form a specific structure and structural limitations are common [19]. Other 3D printing techniques, such as stereolithography (SLA), in which a deflected laser beam or a projected light source is used to cure exposed areas of photopolymer [3] are also used for biomedical applications. This allows a greater versatility in terms of choice of photopolymer available for SLA 3D printer. Other advantages of SLA printing are high accuracy and precision, and fast curing speed, making SLA printing a great tool for generating tissue engineering scaffolds. Commercial SLA 3D printers are typically very expensive. However, open source desktop SLA 3D printers (like LCD 3D Printers) are now available at significantly lower cost [20]. This has opened the power of SLA manufacturing to a wider audience, and hence a greater choice in photocurable polymers and resins are gradually becoming available for biomedical applications [21].

There are essentially three main groups of biomaterials used for tissue engineering applications, ceramics, synthetic polymers, and natural polymers [4]. Each biomaterial has its own advantages and disadvantages, therefore the optimal biomaterial for a tissue replacement depends much on desired application. Numerous synthetic

polymers have been reported as biodegradable and biocompatible biomaterials for tissue engineering applications in the literature. The most commonly used are the polymers poly (lactic acid) (PLA)[22], polyglycolic acid (PGA), poly-dl-lactic-co-glycolic acid (PLGA)[12], polycaprolactone (PCL)[23] and poly(3-hydroxybutyrate) (PHB) [4]. While most of these materials have had much success, due to its tailorable architecture and degradation rates, these polymers also have their disadvantages. For example, inferior mechanical properties (low elongation) and unsatisfactory biocompatibility with cell and tissues (high inflammatory response) [24, 25].

A biomaterial that has been increasingly used for biomedical applications is Poly (glycerol Sebacate) (PGS), first developed in 2002 [26]. The material was described as a tough biocompatible elastomer, inexpensive and with excellent biocompatibility [26]. PGS has been successfully used in a variety of tissue engineering application including replacement of cardiac muscle [27], nerve [28], skin [7], retina [29], and cartilage [30], as well as in drug delivery applications [31], and hard tissue regeneration [32]. Furthermore, the mechanical properties of PGS, and its degradation rates can be tailored to a desired application by controlling its curing time, curing temperature, reactant concentration and its degree of acrylation [26, 33]. Moreover, the elastomer can be totally reabsorbed into the body and its degradation products can be eliminated through natural pathways [34]. PGS has elastomeric properties, and can sustain large deformation without permanent changes in its structure or mechanical properties [32]. Those properties are very desired on the replacement of soft tissues. However, PGS suffers from manufacturing limitations due to high temperatures, high vacuum pressures, and long processing hours [26].

A recent discovery is the acrylation of poly (glycerol sebacate), resulting in a new type of materials called PGSA, which is a photocurable material in presence of a photoinitiator [33]. This modification permits photopolymerization of PGSA, and significantly decrease its curing time. This approach thus provides the opportunity to overcome limitations of PGS manufacturing process. Additionally, this acrylation process also allows for increase in its mechanical properties by increasing its degree of acrylation [33].

Another important aspect to be considered when designing a scaffold for tissue regeneration is the cytotoxicity. The scaffold must not contain any cytotoxic element that can cause the cells to necrose and apoptosis [2]. Typical sources of cytotoxicity consist of initiators used in photopolymerization, macromolecules on the scaffold, solvent residue from polymer synthesis, and degradation products of the polymer.

Photoinitiators directly influence the cytotoxicity of the scaffold and its biocompatibility are very important [35]. The most common photoinitiator used in tissue engineering is Irgacure 2959, since it is the least toxic of Irgacures [35]. However, the peak absorption wavelength of this photoinitiator is from 257-276nm, limiting its use to ultraviolet (UV) light sources. Other photoinitiators were studied and showed promising cytotoxicity. LAP (lithium phenyl-2,4,6-trimethylbenzoylphosphinate), which has a peak wavelength of 375nm, was proven to be water soluble and more biocompatible than Igracure 2959, with the possibility to initiate using visible blue light due to absorptions higher than 400nm [36]. Another biocompatible photoinitiator that is activated using UV light is the Azobis [2-methyl-N-(2-hydroxyethyl) propionamide] (VA 086) with peak absorption wavelength at 385nm. This photoinitiator is water soluble and it its

photodissociation was shown to be noncytotoxic [37, 38]. However, this photoinitiator has a narrow activation range, and if 3D printing with seeding cells, the use of UV light source on photocrosslinking techniques will expose the cells to UV light, which can induce DNA damage and apoptosis of the cells [37].

The next photoinitiator studied with a visible light absorption (peak at 515nm) is Eosin Y disodium salt [38-40]. Eosin Y is very biocompatible, less toxic than Irgacure 2959 and by using visible green light, it is much safer for long term cell functionality [38]. Unfortunately, a co-initiator such as triethanolamine (TEOA) is required to generate enough radicals to produce enough functional group conversion [38, 40].

In this study, it is shown that it is possible to 3D print PGSA using an LCD 3D Printer. This method of 3D printing is fast, simple and provides excellent resolution. The material characterization, biocompatibility, swelling, rheology, and the mechanical properties of the polymer were investigated and presented below.

1.1. Goals for this study

In this study, the strengths of PGSA were exploited to successfully manufacture a tough biodegradable elastomeric material samples using LCD 3D printing. For a successful tissue scaffold to be created, the material must be biologically compatible, chemical and mechanical properties must work well with the 3D printing process, the scaffold must match real tissue properties, and eventually must biodegrade safely in the body. Figure 1 shows a schematic of the iterative process required to develop this 3D printing method. Therefore, combining LCD 3D printing and PGSA is a very promising tool for biomedical applications by allowing the production of complex biocompatible,

elastomeric tissue scaffolds that can be highly customized without modifying the manufacturing process. This method of 3D printing is inexpensive, is a simple and user-friendly process, and provides the option to easily change light sources for the desired application.

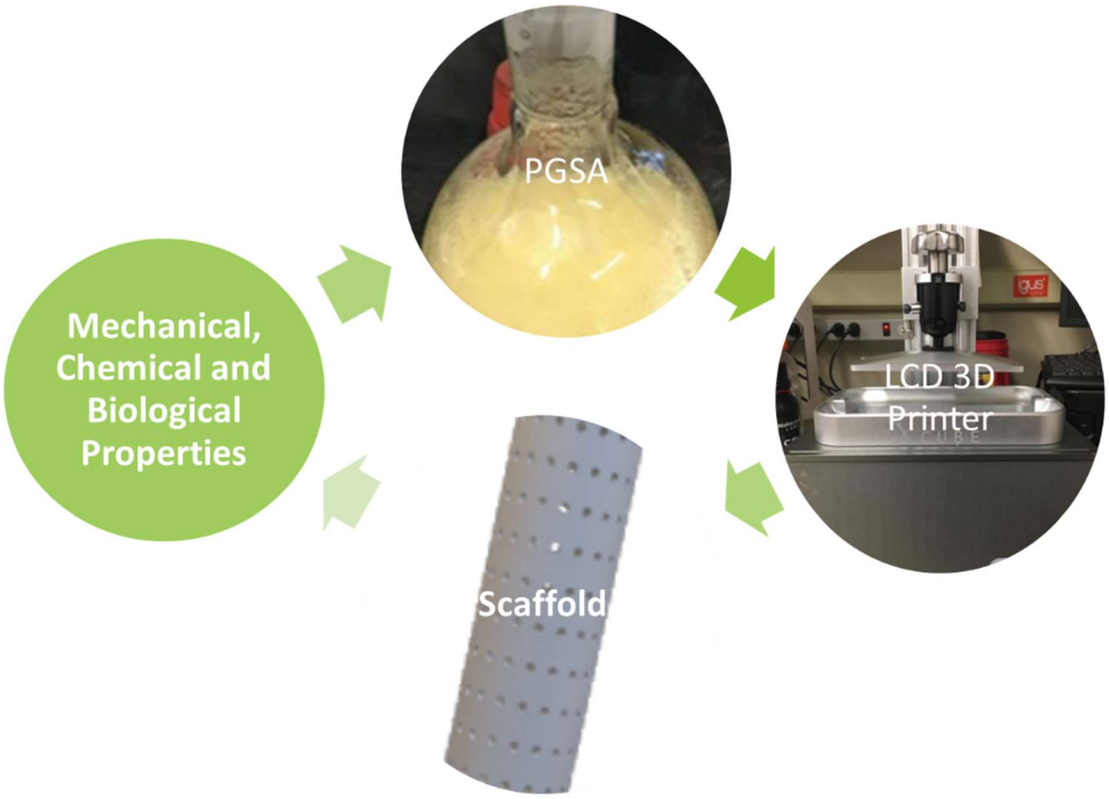

Figure 1. Iterative process to develop a successful scaffold

2 BACKGROUND AND LITERATURE SURVEY

The following paragraphs will provide background information on epithelial regeneration, focused on skin tissue, on the material used in this project, PGSA, and on Microstereolithography. First, the necessary background in skin regeneration is presented, highlining the most recent advances on 3D printing scaffolds for skin regeneration. Then, the most significant advances on PGS and PGSA are also

summarized in this section, presenting the important results obtained by leader groups in the field. Finally, a summary on Microstereolithography is presented, to give the readers background information on 3D printers and explain the reasons of why some of the design decision that were made in this project.

2.1 Epithelial Tissue Engineering

As the largest organ in the human body, the skin serves as the primary barrier to the outside environment, also helping with thermoregulation and hydration retention [41]. The skin has the ability to selfheal, sensory detection and immunity surveillance [42]. Underlying organs have the protection of the skin from pathogens and microorganisms [43]. However, the skin is unavoidably exposed to injuries, such as burns, trauma and chronic ulcers [7]. Sometimes, these wounds are too deep to repair itself and skin grafts or surgical repairs are needed. The goal procedure in these situations is a skin graft, which has some limitations regarding donor shortages, scar formation, pain, and other long-term complications [44].

Epithelial lines both the external skin and inside cavities and lumina of bodies. The skin is essentially composed of three layers presented in Figure 2. The outermost layer is the epidermis, which acts as a barrier on top of the dermis. It is avascular and consists of 95% of keratinocytes [45]. The middle layer is the dermis, the thickest part of the skin, it consists of thin collagen fibers, with collagen, elastin and reticular fibers [45]. On this layer, the fibroblasts are the main cellular component responsible for secreting collagen and proteoglycans, but other cells such as melanocytes (pigmentation of skin) and Langerhans cells (defending against microbes) are also present [45]. Moreover, in between these layers, there are stem cells and epidermal basal cells that are responsible

for the regeneration of the epidermis [45]. The hypodermis is the inner layer responsible for the thermoregulations of the system. It is made of loose connective tissue and lipid moieties [45]. The epithelial tissue also lines the inside of the mouth, the esophagus, the vagina, and part of the rectum. Other epithelial cells line the surface of the cornea, the inside of the lungs, the inner lining of blood vessels, the gastrointestinal tract, the reproductive and urinary tracts, and both exocrine and endocrine glands [46].

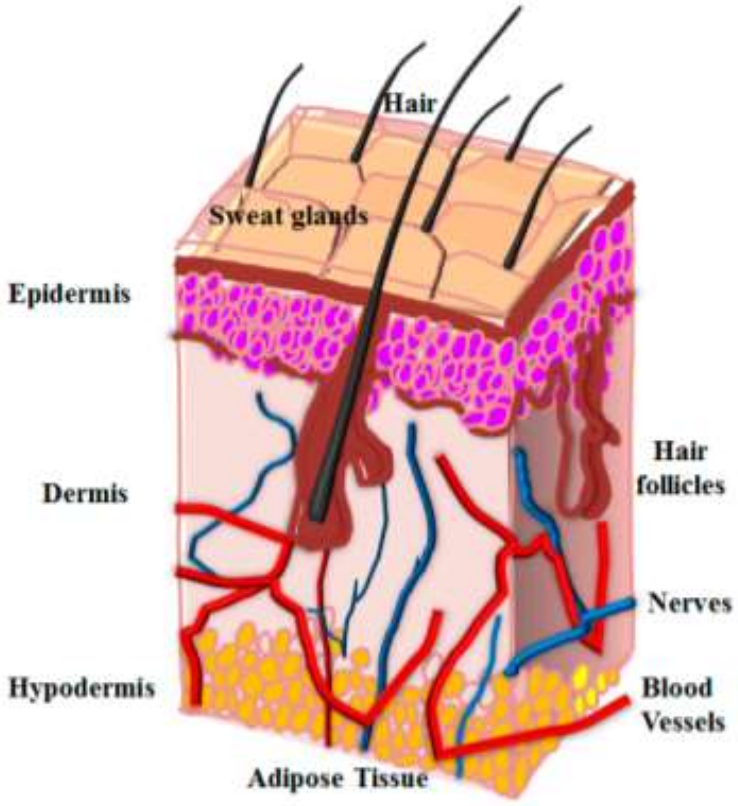

Figure 2. Schematic representation of the three layers of the skin [45]

Over the past few decades, skin regeneration has advanced significantly, evolving from simple epidermal and dermal equivalent to complex bi-layered skin substitutes [47]. Multiple materials and techniques have been used in skin tissue engineering, including both natural and synthetic materials. The list includes collagen [48, 49], chitosan [50, 51],

alginate [50], hyaluronic acid (HA) [52], polylactic acid (PLA) [22] and polycaprolactone (PCL) [53]. However, there is an unmet need for skin regeneration that these materials still cannot provide.

Type I Collagen is the most commonly used material in skin tissue regeneration as a hydrogel. However, it has variable degradability, risks of infection due to its immunogenicity with low homogeneity and repeatability, with additional contraction problems. Alginate has slow degradation rates, poor mechanical integrity, but great biocompatibility [50]. PLA is well known for its high strength and stiffness; however, it generates acidic environments during its degradation process [54]. PCL also presents slow degradation and reabsorption rates [23].

Moreover, multiple techniques have been explored to produce the skin grafts needed for skin regeneration. The recent advances of 3D Printing has emerged as a flexible tool, with the possibility of printing cells and desired biomaterials in a desired path with high precision [55]. There are two main strategies used in 3D bioprinting skin for wound healing. The first is in situ bioprinting, which consists of printing full thickness wound of nude mice using fibrin-collagen layers with derived stem cells or human fibroblasts and keratinocytes [56]. Although these results were promising, further optimization is still required before human trials [56]. The second approach consists of in vitro production, followed by in vitro and in vivo testing. The first group used a free-form fabrication (FFF) to deposit layers of crosslinked collagen with human fibroblasts or keratinocytes [57, 58]. The second group used laser assisted bioprinting (LaBP) to deposit alternating layers, summing to 20 sublayers each of immortal murine fibroblasts and immortal human keratinocytes embedded in collagen matrix [59, 60]. However these methods have

a few drawbacks of now using human primary cells, the skin produce does not have the structural quality of the normal skin, and the duration of the process is still far from the desired range [61]. Recently, Cubo and his group in Spain developed an FFF 3D bioprinting to create a engineered human plasma-derived fibrin matrix bilayer skin using human fibroblasts and human keratinocytes [61]. They showed the most promising results, with structural and functional characteristics as well as appearance and consistency [61]. According to the literature, this is the closest of a functional skin engineered so far, but there are still limitations to overcome.

Considering the disadvantages of the biomaterials presented above, from most materials used in skin regeneration, newly materials have been developed and explored to fulfil these requirements. PGS and PGSA have interesting properties that can be very useful in skin tissue engineering. For a successful tissue skin replacement, scaffolding materials should be tough, with fast rates of biodegradability and very biocompatible. PGSA fulfills these characteristics and also adds the tailorable mechanical and degradation properties according to the desired application, with an additional control over the porosity of the desired shape [7]. PGSA also presents better mechanical integrity than commonly used hydrogels, with great biocompatibility and hydrophilicity. Therefore, PGSA scaffolds can be a very promising tool for skin tissue engineering combined with 3D bioprinting technologies.

2.2 Polymer Synthesis and Characterization of PGS and PGSA

There are essentially two main groups working on the development of PGS and PGSA. Langer's group, besides developing the biomaterial itself, is working on different application using both PGS and PGSA [10, 26, 29, 33, 34, 62-65]. Burdick group has

been working on the development of PGS and PGSA since 2008 [66, 67]. Recently his group published one article about 3D printing photocurable PGSA and another about 3D printing norbornene-functionalized PGS, both using an FDM 3D printing method [68, 69]. The significant results of their work are summarized on the following sections.

2.2.1 Synthesis of PGS prepolymer and PGSA

The traditional synthesis process of PGS has two phases. The first phase is the prepolymer phase which consists of the polycondensation of an equimolar amount of glycerol with sebacic acid at 120°C for 24 hours, under presence of argon and a pressure of 1 torr. Then, the pressure is reduced to 40 mtorr after 4 hours, and kept it for an additional 48 hours to conclude its crosslinking phase. After this stage, the polymer becomes a thermoset, meaning that the material cannot be modified by re-heating [26]. Wang used molds and salt leaching processes to create PGS scaffolds [26]. In this process, after the prepolymer is complete, PGS is dispensed into a mold with salt, and the curing procedure is continued until its crosslinking phase is finished. This process results with a porous scaffold, and the salt is then removed by dissolving the scaffold into deionized water. The biomaterial was also shown to have tough elastomeric characteristics [26].

The acrylation of PGS was further introduced in 2007 by Nijst [33]. The acrylation of PGS provided an extra level of control of the mechanical properties of PGS. The synthesis process of PGSA consists of the PGS prepolymer being dissolved in anhydrous methylene chloride and cooled to 0°C under nitrogen flow for 10min. An equimolar amount of acryloyl chloride and triethylamine were added into the solution and then stirred at room temperature. 4-methoxyphenol was added to the reaction solution

and methylene chloride was removed using a rotary evaporator. Ethyl acetate was used as a solvent and the solution was vacuum filtered to remove TEA salts. Ethyl acetate was then removed using a rotary evaporator resulting on a viscous liquid, which was then dissolved in methylene chloride and stored at 4°C. The photo-initiator 2,2-dimethoxy2-phenylacetophenone (DMPA) was added to the samples in methylene chloride which was then removed with a rotary evaporator prior to use. Photopolymerization reaction was initiated using an ultraviolet light of 4mW/cm^2 for 10 minutes [33]. The new polymer remained biocompatible, with similar elastomeric properties. Moreover, the biomaterial was photocured by photopolymerization much faster than PGS. Likewise, PGSA kept its ability of tailorable mechanical properties according to its desired application.

2.2.2. Characterization of PGSA

The physico-chemical, mechanical and thermal properties of PGS and PGSA are essential to understanding and selecting a biomaterial for tissue replacement applications. Fourier Transform Infrared Spectroscopy (FTIR) analysis were carried to characterize the chemical structure of the polymer. Wang's studies [26] showed the signature bands for ester linkage of PGS showing peaks at 2930 cm^{-1} and 2855 cm^{-1} for alkaline groups, an intense band at 1740 cm^{-1} for C=0 stretching and at 1164 cm^{-1} due to C-0 stretching [26]. A broad peak at 3475 cm^{-1} was detected and assigned to hydrogen-bonded hydroxyl groups, likely from free hydroxyl groups which are not modified by acryloyl chloride [33]. Additionally, the formation of a polymer network was confirmed by the increase of the band at 2930 cm^{-1}, corresponding to the vibration of alkyl groups, and the elimination of the band at 1375 cm^{-1}, known to be associated with acrylate groups after photocuring of PGSA [33]. The FTIR results from this study is shown on Figure 3.

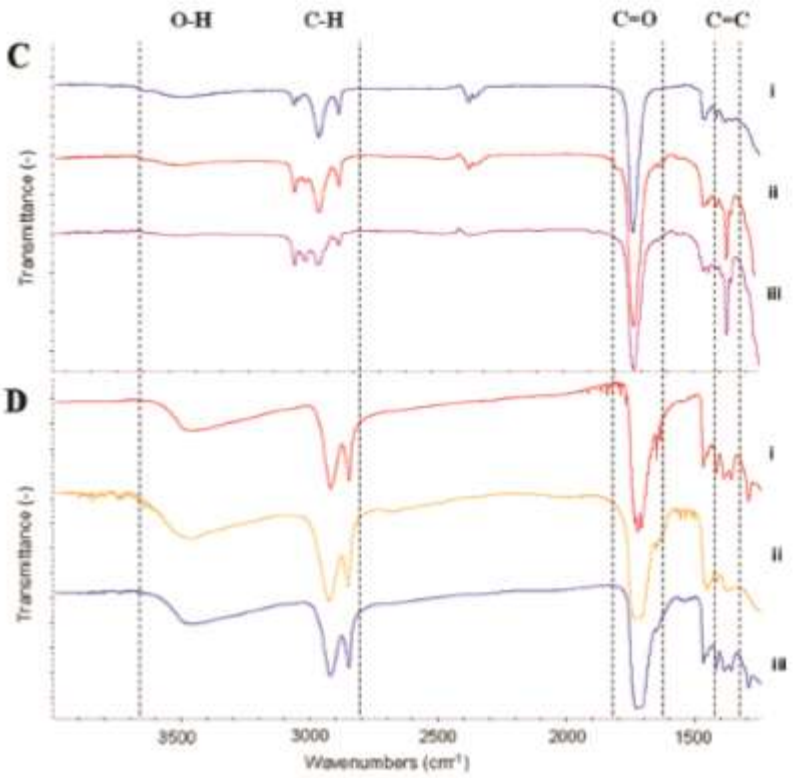

Figure 3. FTIR spectrum of (c)i. PGS prepolymer ii. PGSA(0.2DA); iii. PGSA (0.54 DA); (d) i. thermally cured PGSA ii. Photocured PGSA (0.2DA); and iii. Photcured PGSA (0.54DA)[33].

Another method used by Maliger and his group to characterize PGS was the FT-Raman spectroscopy [70]. Raman spectroscopy analysis determines the presence of functional and end-groups, monomer and polymer structure and conformation, orientation of chains, and to follow changes in structural parameters due to mechanical or environmental stresses [70]. The peaks obtained by the Raman spectroscopy represents fundamental transitions providing chemical information. Maliger [70] characterized the dependence of reaction rate on concentration and temperature using three molar ratios (0.6, 0.8, 1.0) of the reactants concentration, and three different temperatures (120°C, 130°C, 140°C), using a laser of wavelength equal to 1064nm.

The results presented a typical spectrum on the range of 200-3800cm^{-1} at a laser power of 320 mW and at spectral resolution of 8cm^{-1}. The FT-Raman spectrum of PGS with 0.6 molar ratio and at 120°C is shown on Figure 4. The spectra show acid (1642cm^{-1}) and ester (1738cm^{-1}) peaks and similar results were obtained for the other molar ratios and temperature.

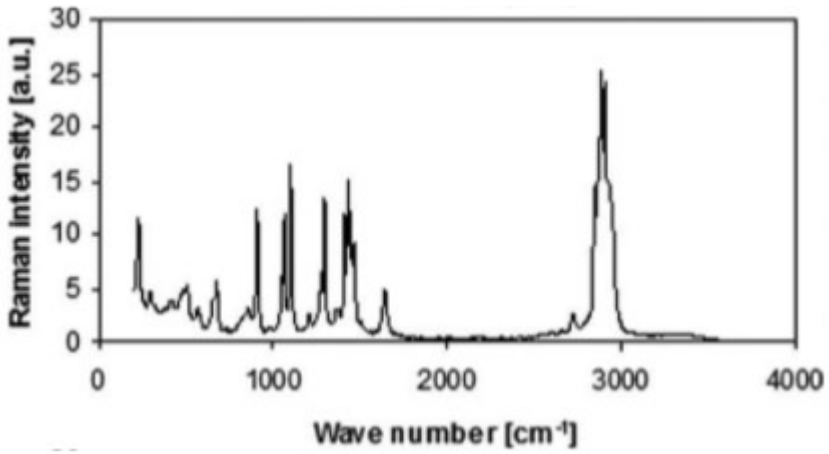

Figure 4. FT-Raman spectrum of PGS at 120C and 0.6 molar ratio [70]

2.2.3 Mechanical Testing

Tensile and compression tests were performed in previous studies to show its viscous elastic behavior, typical for soft elastomeric materials. The typical stress-strain curve of PGS resembles the curve form vulcanized rubber as shown in Figure 5. The PGS and the vulcanized rubber curves are characterized by low modulus and large elongation, representing their elastomeric and tough materials. The opposite can be seen on the P4HB curve, with high modulus and low yield strain, characterizing a stiff material.

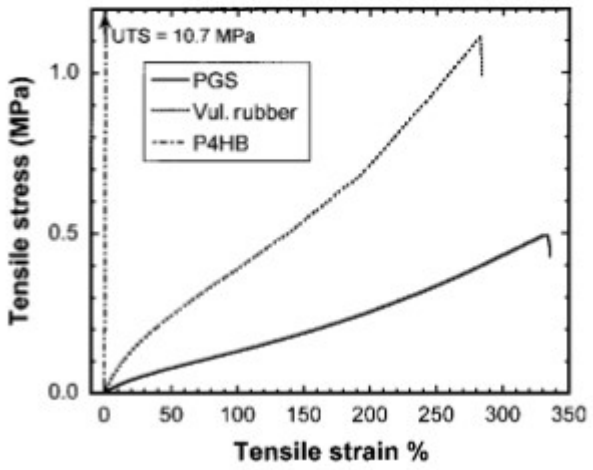

Figure 5. Stress and Stain curves of PGS, Vulcanized Rubber and P4HB[26].

The first experiments showed that PGS has an average tensile Young-Modulus of 0.025 -1.2 MPa, ultimate strength higher than 0.5MPa and strain failure greater than 330% [26, 28, 71]. However, the mechanical properties of PGS and PGSA can be tailored by changes in curing temperature, reactants concentration and degree of acrylation, and can be modified according to the desired application. In the PGSA studies, the degree of acylation was linearly proportional to the Young's modulus and ultimate tensile strength as shown on Figure 6. It was found that PGSA had Young's modulus between 0.05 to 1.38MPa and an ultimate tensile strength of 0.05 and 0.5MPa [33].

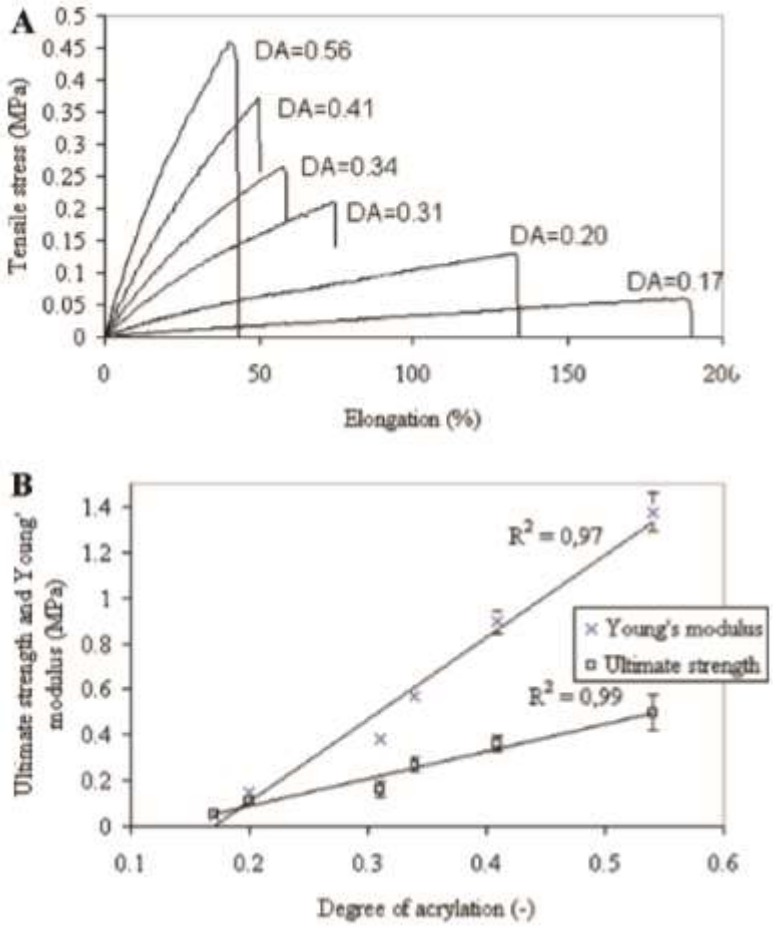

Figure 6. (a) Stress and Strain curve for photocured PGSA with different degrees of acrylation. (b) By increasing the degree of acrylation, the ultimate tensile strenght and Young Modulus also increased linearly [33].

In another study, Gerecht studied PGSA scaffolds for cell encapsulation and culture [10]. The compression modulus of PGSA with 15% extra glycerol and 35% extra glycerol were found to be 119±65kPa and 80.2±28 kPa respectively [10]. The Young's Modulus of Elasticity is reported to significantly decrease after the addition of glycerol. The Young's Modulus was found to be 59.9±4.1 kPa for PGSA with 15% of glycerol and 42.3±5 kPa for 35% glycerol, compared to 568±220 kPa of only PGSA [10].

2.2.4 Thermal Characterization

The thermal properties of PGS were detected using a Differential scanning calorimetry (DSC). The two important properties are essentially glass transition temperature and melting temperature. The first studies by Wang [26] showed two crystallization temperatures at -52.14°C and -18.5°C, and two melting temperatures of 5.23°C and 37.62°C. He also found that the that polymer is totally amorphous at 37°C and that PGS is a thermoset polymer. On Jaafer study, he found that the degree of acrylation of PGS decreases meaningfully with increasing curing time and temperature as shown on the DSC spectra on the Figure 4 below [72]. By analyzing the Figure 7, it can be determined that the recrystallization peak height at -20°C reduced significantly with curing time and temperature. Moreover, the slight discernible sweep between -30 and -40°C represents the glass transition temperature, which was constant with the changes in time and temperature [72].

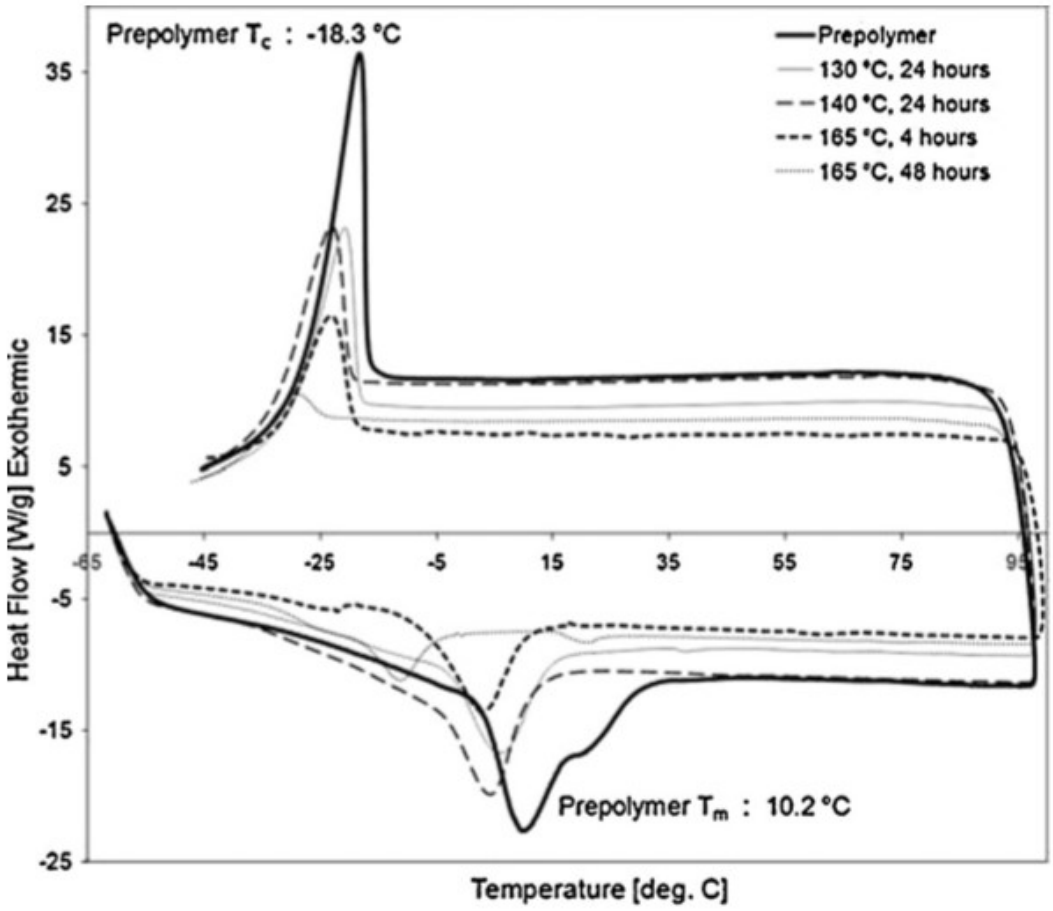

Figure 7. DSC curves for PGS prepolymer at different curing times and temperatures [72].

2.2.5 Rheological Characterization

The rheological properties of PGSA were previously characterized using an AR2000 stress-controlled rheometer (TA Instruments). Dynamic sweeps were performed to find the Storage(G′) and loss (G″) moduli with time under 0.5% strain and 1Hz, as well as the viscosity of PGSA was obtained by the slope of the shear stress versus shear rate plot, under a continuous flow of (0.0–50.0s^{-1}) [68]. The viscosity results are shown in Figure 8. The study demonstrates how the changes in molecular weight can directly influence the viscosity of the polymer.

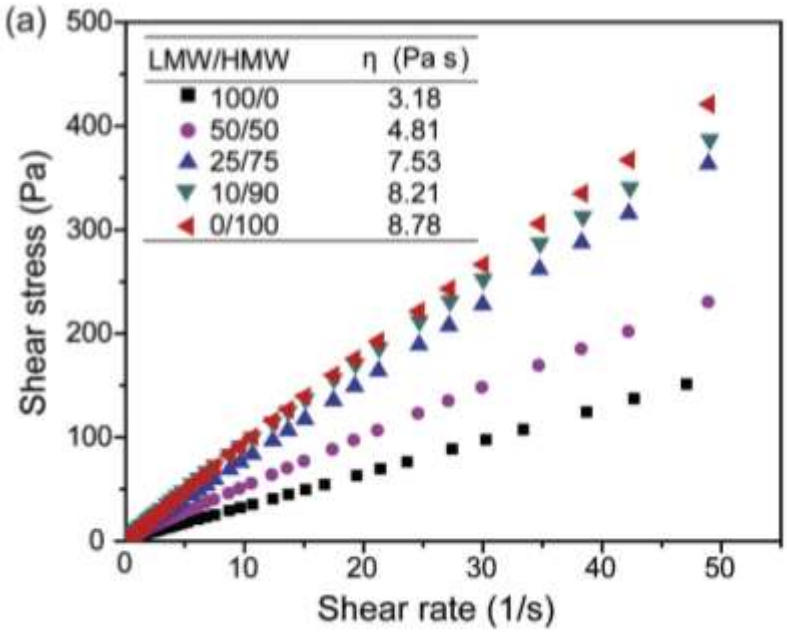

Figure 8. Shear stress-shear rate plots of different ratios of PGSA blends [68]

2.2.6 Scaffold Characterization and Polymer Degradation

To verify the geometry and sizes of the porous structures on the scaffold, typically scanning electron microscopy was used on most of previous leading studies [68]. To obtain the density of the printed scaffold, dimensions were measured, specimens were weighted, and the mass per volume was calculated, and finally compared to solid samples to determine the percent density of the scaffolds.

In a follow on publication [34], the in vivo degradation of PGS was described. The author analyzed the changes in weight, mechanical strength, implant shape, surface, and degree of swelling of PGS and PLG [34]. Additionally, five samples were implanted subcutaneously in 15 female rats. The samples were removed every seven days and rinsed in phosphate-buffered saline (PBS) solution and deionized (DI) water. The results are presented on Figure 9.

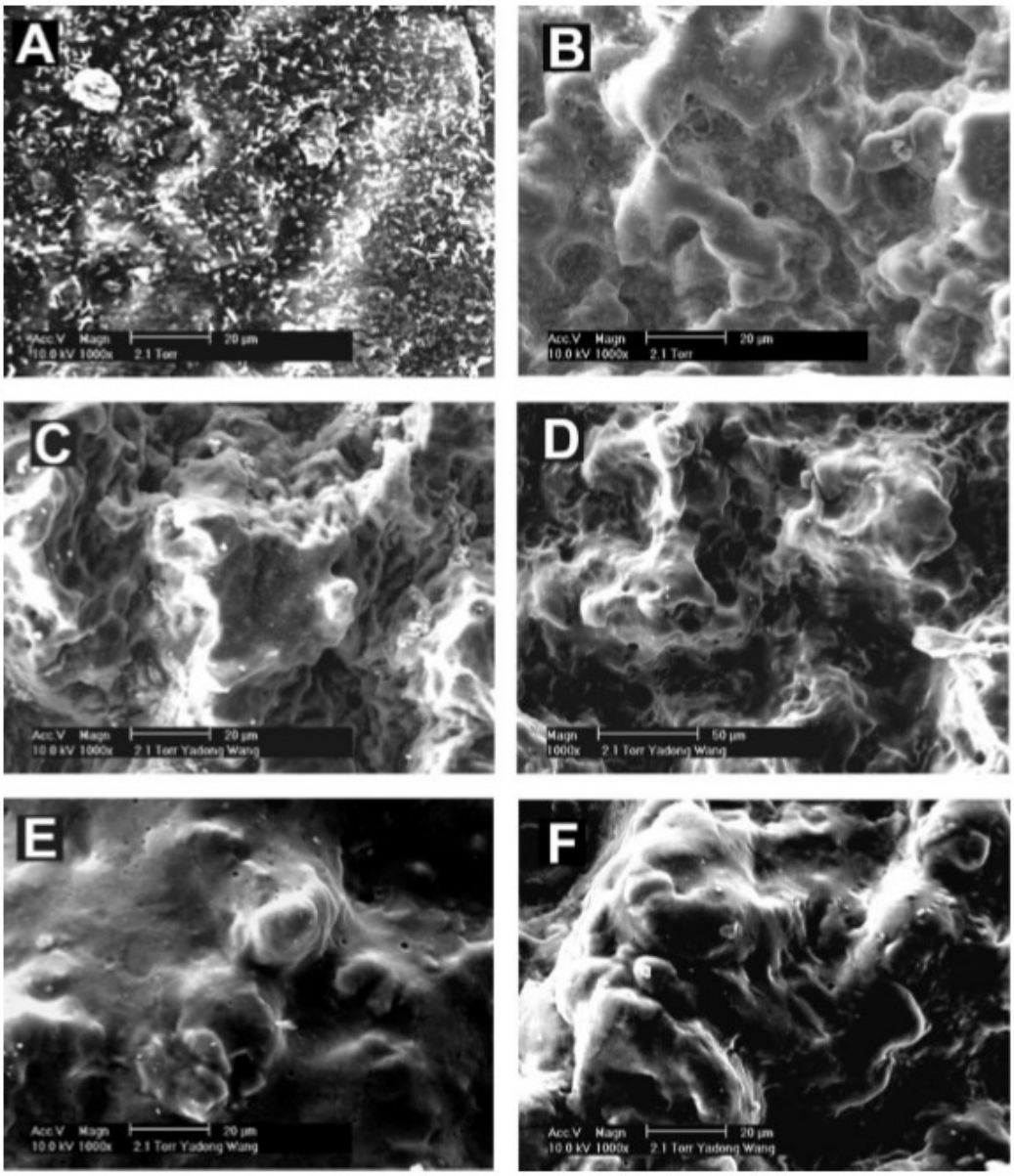

Figure 9. SEM of PGS in vivo studies at various points of degradation. PGS (A) 0 days; (B) 7 days; (C) 14 days; (D) 21 days; (E) 28 days and (F) 35 days [34].

The conclusions of this study were that PGS degrades by surface erosion, showing a linear mass degradation profile. Macroscopically PGS implants maintained their geometries, and microscopic observations showed that the PGS surface maintained its integrity, it preserved its shape and most of its mechanical strength, besides not presenting any surface cracks. For the degree of swelling, the amount of water increased

linearly, and after 35 days, when the polymer had degraded steadily by 70% of its mass, its water content was 15% [34]. Figure 10 describes the findings of the study.

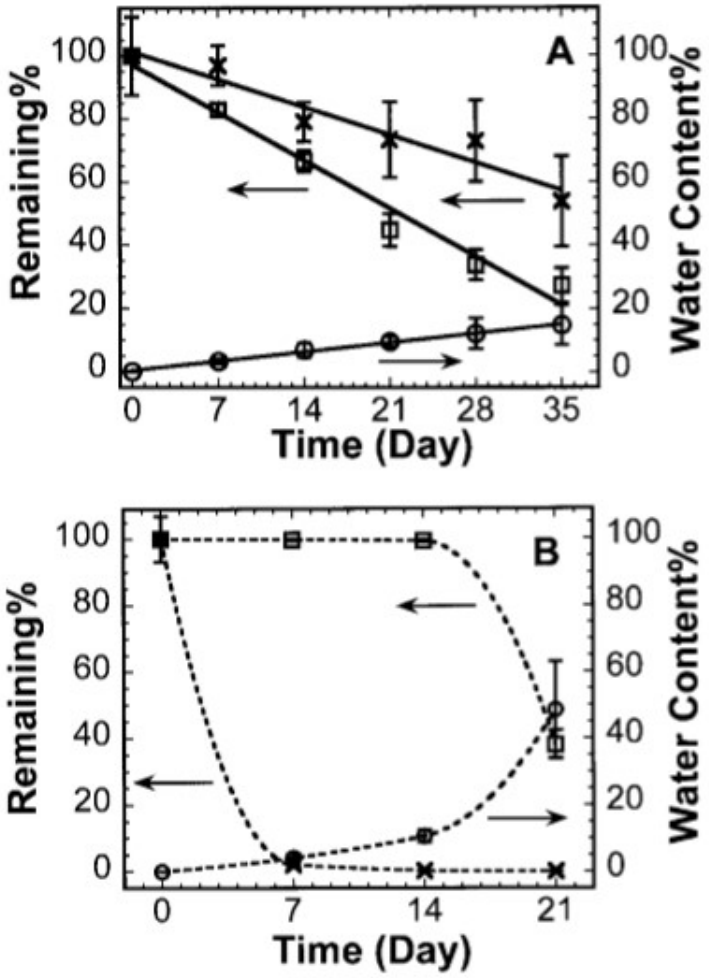

Figure 10. Assessment of the changes in mass (square), mechanical strength (X), and water content (circle) of PGS (solid line) and PLG (dashed line) implants upon degradation. (A) Steady changes of PGS. (B) Abrupt changes of PLG [34].

In vitro degradation was obtained by enzymatic degradation study [33]. The samples were placed on a phosphate-buffered saline (PBS) solution, with bovine pancreatic cholesterol esterase (40 units/mL) and incubated at 37 °C. The samples were removed, washed on deionized water and then dried at 90 °C for 7 days and weighed again to control the mass loss [33]. He found that the PGS samples degraded 15% in 10

weeks in PBS and 6 weeks in vivo. Similarly, PGSA only degraded 10% after 10 weeks [33].

In two other studies [66] and [68], the degradation of PGSA scaffolds were characterized following a similar process. According to Ifkovits study, the samples were placed on a mold, cured, photocured and constructed on the shape of a disk (1mm thick, 5 mm diameter). The results of his study are shown of Figure 11.

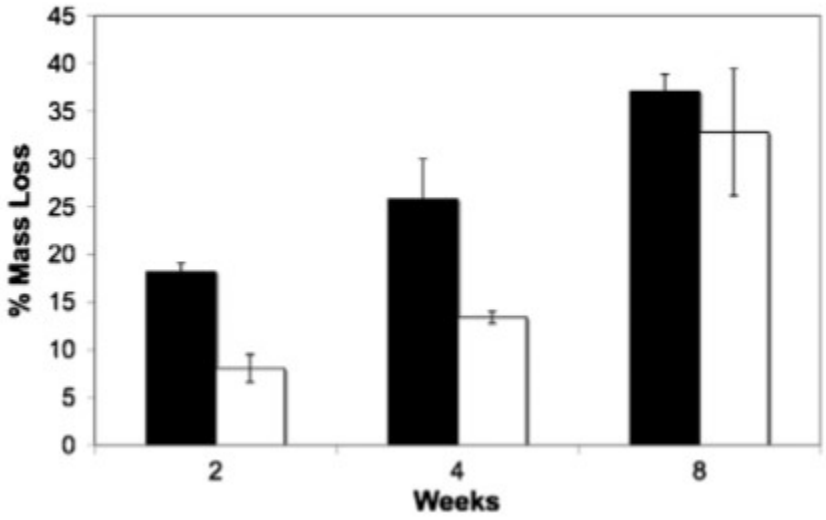

Figure 11. In vivo (black) and in vitro (white) degradation results at 2, 4 and 8 weeks [66].

In [68], the samples were 3D printed with various densities and in the shape of disks (1mm thick, 3mm diameter), weighted, and incubated in 1.5ml of phosphate-buffered saline (pH 7.4), and placed on an orbital shaker at 37°C for up to 8 weeks [66, 68]. The solution was replaced weekly with fresh phosphate-buffered saline. Every two weeks, three samples were removed, lyophilized and weighted to control the mass loss. As expected since PGS degrades by surface erosion, the material lost only 20% of their mass during the 8-week period and the results are presented on Figure 12.

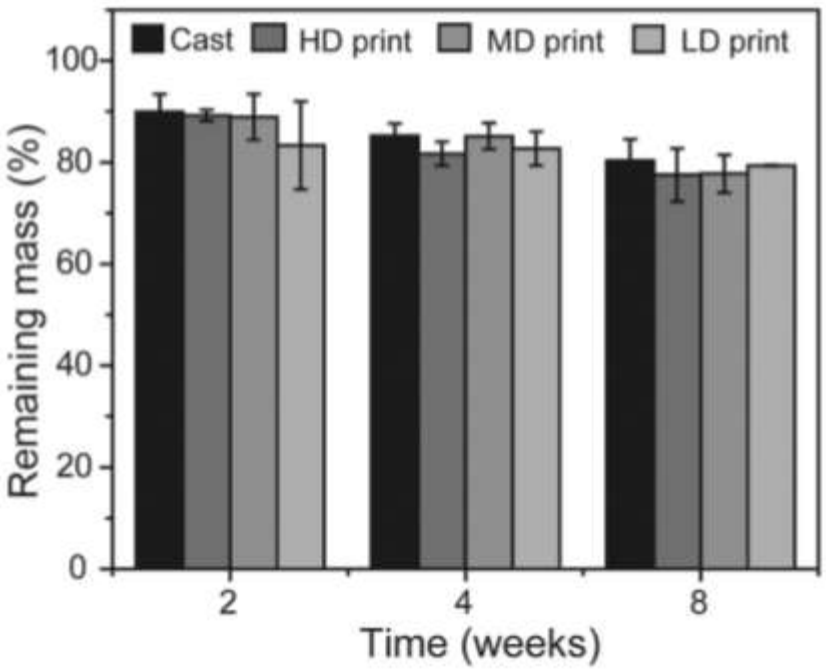

Figure 12. Degradation profile of PGSA scaffolds in PBS at 37°C after 8 weeks. From Ref. [68]

2.2.7 Cell Culture and Biocompatibility

Biocompatibility tests were also performed, and it was concluded that PGS is biocompatible both in vitro and in vivo. Most of the studies used NIH 3T3 fibroblast cells[26, 49, 68, 73]. Yeh used the same cells and cultured it under a 37°C humidified atmosphere of 5% CO_2 in high glucose with 10% fetal bovine serum and 1% penicillin/streptomycin [68]. 3D printed scaffolds were sterilized by incubation in ethanol for half an hour, washed with PBS, and incubated in serum-containing media for 24 hours [68]. Their initial tests used 3T3 cell suspensions dripped into the PGSA scaffold in a 24-well cell culture plate to test cell adhesion and viability. After 24h, the scaffolds were transported to new well sand stained with calcein-AM at room temperature for 20 minutes [68]. To verify cell proliferation, 3T3 cell suspensions were dripped in the top center of the PGSA scaffolds (10 layer, 10x10mm with height of 1.45mm), in a 24-well

cell culture plate [68]. The specimens were incubated for 2 hours and 2mm of culture medium was added. Then, the scaffold were transferred to a new plate after 24 hours to assess the metabolic activity after 4 days using an Alamar blue assay according to the manufacturer's protocol (Invitrogen Biosource,USA) [68].

Cytocompatibility is essential to prove that 3D printed PGSA scaffold can be successfully used in tissue engineering and showing that the same scaffold can promote cell growth and proliferation. Yeh's results showed that the fibroblasts were viable and spread into continuous layers onto the 3D oriented scaffold [68]. These results were expected according to previous findings on cell adhesion of PGS [74]. Yeh also used an Alamar blue to assay the cellular metabolism, he observed an increase in the number of fibroblasts for the 3D printed PGSA scaffold over time. On the second day, the cell population doubled and continued to increase up to the fourth day, as shown on Figure 13 [68]. Therefore, he concluded that the 3D printing process did not affect the PGS cytocompatibility.

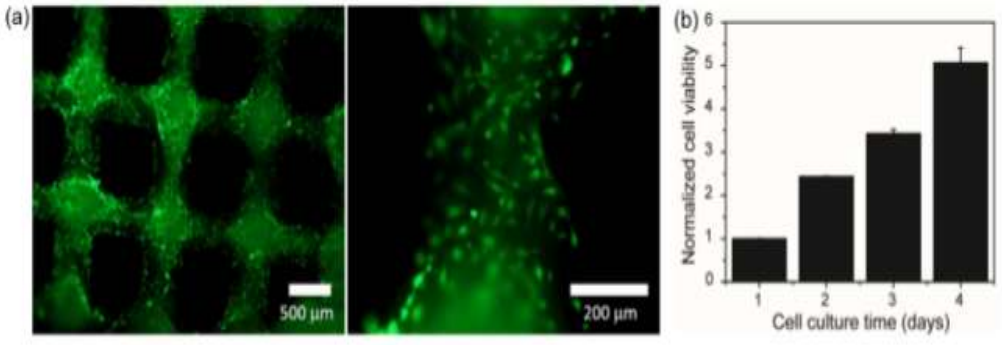

Figure 13. (a) 3T3 fibroblasts cultured on a 2-layered scaffold and stained with calcein-A Mafter culture for 24 hours. (b) Normalized cell viability of 3T3 fibroblasts cells on a 10-layered 3DP scaffold. From Ref. [68]

2.3 PGS Applications

PGS is a known synthetic biocompatible material proposed originally for soft tissue engineering. However, over time, because of its desirable properties, this biomaterial has attracted more attention, with applications varying from scaffold material for both soft and hard tissue replacement, tissue adhesives, and drug delivery systems applications [75].

2.3.1 Cardiac Tissue Engineering

One of the main causes of myocardial infarction is the cell death produced by ventricle expansion [74]. Common strategies to treat heart failure are cell therapy, and cardiac patches for cardiac support. Chen provided an innovative treatment strategy for heart failure using PGS augmented with cardiomyocytes [76]. He observed that unless willingly interrupted, the active cell cardiomyocytes continued beating continuously for more than three months [76]. Moreover, in vivo tests showed that the cardiac patches remained stable for two weeks without any loss of the ventricular function [76]. Therefore, PGS provided mechanical support for the cardiac cell with cell delivery.

Moreover, to improve the properties of engineering cardiac tissue, pre-treatment of PGS with fibroblasts was performed by Radisc [63]. The study showed that the cardiac fibroblasts were successfully recovered and that the PGS scaffold provided a similar ventricular environment and support for the cardiac tissue [63]. Furthermore, the in vivo studies using rat models showed that the scaffold was vascularized, and the results are presented on Figure 14. Therefore, PGS has great potential for cardiac tissue replacements.

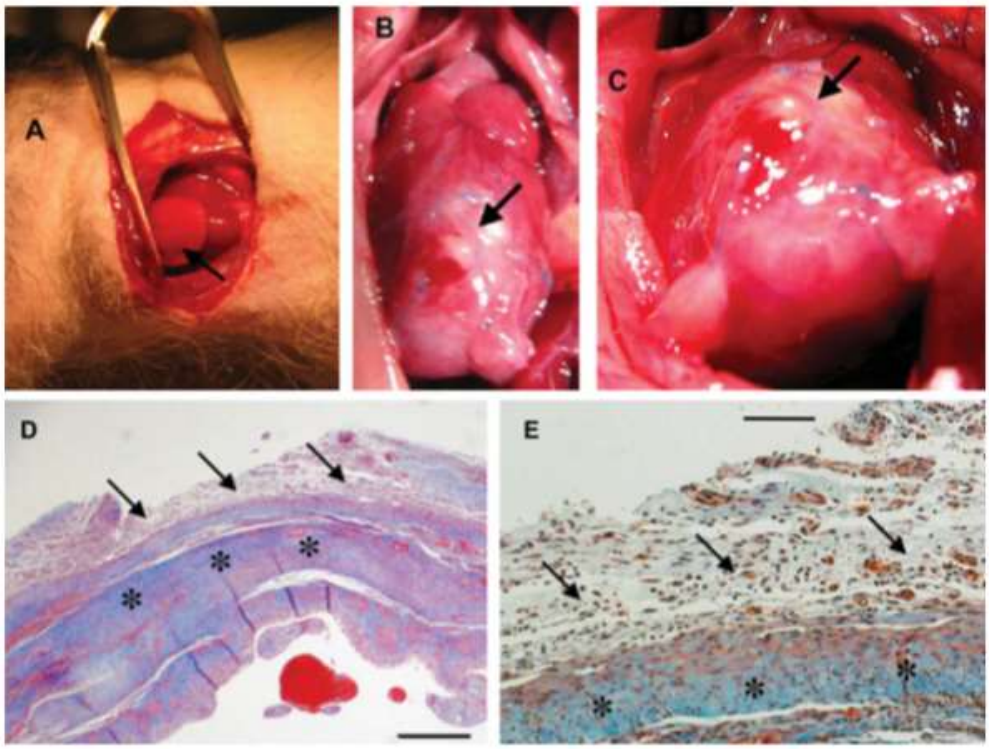

Figure 14. In vivo results of PGS scaffold in a rat heart infarction model. According to results of Radisc,[63] (A) Implantation of the scaffold. (B and C) Macroscopic view of the same are after 2 weeks of implantation. (D) Cross-sectional area of the graft-host interface after 2 weeks. (E) Higher magnitude of image D showing excellent integration between the graft (arrows) and the host (stars). Scale bars: 0.5mm (D) and 100μm (E). From Ref. [63]

2.3.2 Cartilage Tissue Engineering

One of the most challenging tissue to replicate is cartilage tissue. Mostly due to its complex extracellular matrix designs as well as its viscoelastic properties. This tissue can withstand multiple loading cycles (on the joints), providing minimal wear as well as demonstrating elastic characteristics, such as in the nose and ears [32]. Depending on the location and extent of an injury, articular cartilage can selfheal. However, some tissues lack vasculature, with almost no capacity to repair itself. Therefore, the use of tissue engineering to repair cartilage tissue has been widely explored.

One of the first attempts to use PGS scaffold for cartilage tissue engineering was performed by Kemppainen and Hollister [30]. They used free form techniques to generate a 3D PGS scaffold. The results showed that PGS has the capability to produce cartilaginous matrix [30]. Another study carried out by the same authors showed that the PGS scaffolds were still able to promote chondrocytes to proliferate. However, in this study, there was also formation of a gene expression for cartilage elimination and ossification [23].

2.3.3 Retinal Tissue Engineering

The retina is an eye tissue that converts light into electrical signals using photoreceptor cells. These signals go to the brain to be interpreted and images are eventually created. Diseases that can degenerate this tissue are very difficult to be cured, affecting the photoreceptor functions, and no cures have been found yet. However, alternative methods to replace the damaged photoreceptor cells have been created [29]. The successful membrane selected to replace retinal tissue should be biodegradable, inserted into the subretinal space to induce specific photoreceptors to be eliminated, or scaffold to support and proliferate the photoreceptors cells [29, 64]. Moreover, the material must have similar mechanical properties to the retinal tissue, with high flexibility, large elongation, and with a scaffold designed to cell attachment and proliferation, without producing any toxicity.

Thus, PGS membranes were developed. One of the most promising study using PGS on this application was the creating of a PGS scaffold for photoreceptor cells delivery [29, 64]. The study showed high potential to target distribution of progenitor cells to the retina and endorsed cell differentiation [64]. Even though there is limited data

available, the results were very promising for PGS membranes to be used in retinal tissue replacements, due to its tailoring properties, high compatibility with photoreceptor cells and high cell differentiation rates [29, 32].

2.3.4 Nerve Tissue Engineering

Various biomaterials have been studied so solve problems related to nerve tissue engineering. Most of the synthetic materials presented exhibit unfavorable swelling and inflammatory responses. Therefore, due to its biocompatibility characteristics, PGS was selected to be explored for nerve tissue engineering [28]. Several in vitro tests using Schwann cells and in vivo compatibility tests were performed on rats. The in vitro tests were positive, showing biocompatibility with minimal toxicity [28]. In vivo tests showed that PGS demonstrated less inflammatory response and fibrosis than the commonly used poly(lactide-co-glycoilide) (PLGA), with no swelling detected. Therefore, it could be concluded that PGS is a promising material for neural reconstruction applications.

A recent study published in 2017 presented a modified PGS using atom transfer radical polymerization with methyl methacrylate so that the polymer could be electrospun into nanofibers for electrospinning. They also added gelatin into the copolymer to increase its hydrophilicity and biocompatibility. It was found that the PGS-based nanofibers promoted cell proliferation for nerve regeneration [14]. Therefore, the authors concluded that this new PGS-based copolymer can be a new promising tool in various tissue engineering applications [14].

2.3.5 Skin Tissue Engineering

Recently, PGS elastomer scaffolds were fabricated using particulate leaching techniques for skin tissue regeneration [7]. As mentioned earlier, since the conventional

materials used in skin regeneration still cannot satisfy the essential needs of skin tissue engineering, PGS and PGSA show promising advantages such as great biocompatibility, fast tailorable degradation rates, and sufficient mechanical integrity as it is an elastomer.

As a significant property in tissue engineered scaffolds, the porosity was essential to improve the water uptake of PGS. Zhang also used the porous structure of the scaffold to control degradability of the polymer, which it is of great importance in skin tissue engineering [7]. The feasibility of these scaffolds was tested using mouse dermal fibroblasts (MDFs) on the scaffold. The results showed good cell attachment, proliferation and deep penetration of MDFs into the scaffold, confirming the biocompatibility of the material [7].

2.3.6 Hard Tissue Engineering

PGS elastomeric properties were also desired on hard tissue engineering mostly involved with bone replacement. PGS was previously investigated for this application in combination with various composites materials [77]. However, a series of papers published investigated the mechanisms inducing bone formation with PGS [78, 79]. In the first study, the quantity and quality of the bone regenerated using microcomputed tomography and by four-point bending flexural tests after 8 week implantation [79]. It was concluded that PGS's lower stiffness allowed load-transducing, where bone deposition and maturation takes place [79]. Therefore, PGS elastomer can be an osteoconductive material with much potential for regeneration of bone. I the second study, PGS was characterized for its mechanical properties (with cyclic compression loads), biocompatibility with osteoprogenitor cells, and in vivo regenerations effects [78]. The PGS scaffolds were also compared with a common biomaterial used in this

application called poly lactic-co- glycolic-acid (PLA/PGA). This study concluded that PGS is osteocompatible and was great with bone regeneration and transmitting mechanical signals to adjacent cells, promoting cell differentiation and matrix maturation to proper bone remodeling [78].

2.3.7 Tissue Adhesive

It is difficult to find biomaterials that can sustain mechanical deformations while still adhering to the tissue. The traditional methods used in medicine today, sutures and staples, do not have highly elasticity properties, and can produce inflammatory responses to the tissue and toxicity. Therefore, the properties of PGS became so attractive to the tissue adhesives applications. In 2008, Mahdavi showed a new generation of tissue adhesives using PGSA, to produce an adjustable elastic product and minimal tissue response [65]. Therefore, PGSA has much potential in the tissue adhesive, with many practical applications on the surgical world.

2.3.8 Drug Delivery

Controlled drug delivery has multiple advantages over conventional delivery drugs. It allows the possibility of a target site, continuous maintenance, with reduced toxicity [31]. The possibility of integrating drug delivery with tissue engineering applications allows a great advantage for local drug delivery [80]. Using a scaffold as a delivery vehicle is crucial for a delivery because the biomaterial has a strong influence on the drug encapsulation and its release. Additionally, the material must be biocompatible and biodegradable.

This approach has been used for anti-cancer therapies. PGS implants were used as drug delivery vehicles for anticancer therapy [31]. PGS was selected because of its

tailorable degradability and great biocompatibility. The anti-cancer therapy using PGS consists of delivering the drugs to target cancerous tissues to reduce toxicity [31]. PGS samples were prepared with anti-cancer drugs and went through comprehensive examination involving chemical characterization, in vitro degradation, drug release behavior, in vivo degradation and tissue biocompatibility [31].

In vitro degradation showed that after 30 days the sample maintained their geometry while degrading, and the degradation rate directly increased with increasing the drug concentration [31]. In vivo degradation studies performed intramuscularly on rats exhibited that PGS degraded in a much faster rate when compared to the in vitro degradation, with no notable inflammation, good biocompatibility and no toxicity [31]. Therefore, with the results obtained was possible to conclude that PGS is a great candidate for bioresorbable drug delivery carrier for anticancer therapy.

PGS has also been used in a different study on the treatment of chronic prostatitis [81]. An antibiotic called ciprofloxacin-HCL (CIP) was encapsulated into a tubular PGS and the drug was released via osmosis and diffusion mechanisms. The results obtained from these studies showed that OGS was again successful on delivering the drug to the target tissue acting as a semipermeable material.

2.4 Microstereolithography

2.4.1 Background

With the advances in Additive Manufacturing and the stereolithography 3D printing (SLA) becoming more available, the resolution of these well-established technologies started to improve significantly, with features as small as 75μm on a

photocurable resin using ultraviolet (UV) laser beam [82]. Mask projection microstereolithography is a slight modification of the traditional SLA printing process, which uses a UV light source with a dynamic pattern mask (generator) to pattern the light and expose the entire cross-sectional area at once, differently from the traditional SLA methods that are limited to the laser beam diameter. This type of 3D printer can feature sizes smaller than 10μm while also dropping build times significantly [21, 82-84].

Mask projection microstereolithography consists of a light source, either a lamp, laser or a light emitting diode (LED), passing through a series of optics, such as collimating lenses, wavelength filters, and homogenizing rods. A mirror can be used to guide the light into the dynamic mask that is usually used to pattern the light source into the desired digitally patterns created from a CAD file. Typical dynamic masks include Liquid Crystal Display (LCD) and Digital Micromirror Devices (DMD). Finally, if desired, the patterned light is resized by a series of lenses to focus the final image on the surface of the photopolymer or at the bottom of a vat. The light projected causes the photopolymer to crosslink, causing it to change phases from liquid to solid in polymerization process [82]. Figure 15 shows a schematic of a common mask projection microstereolithography system.

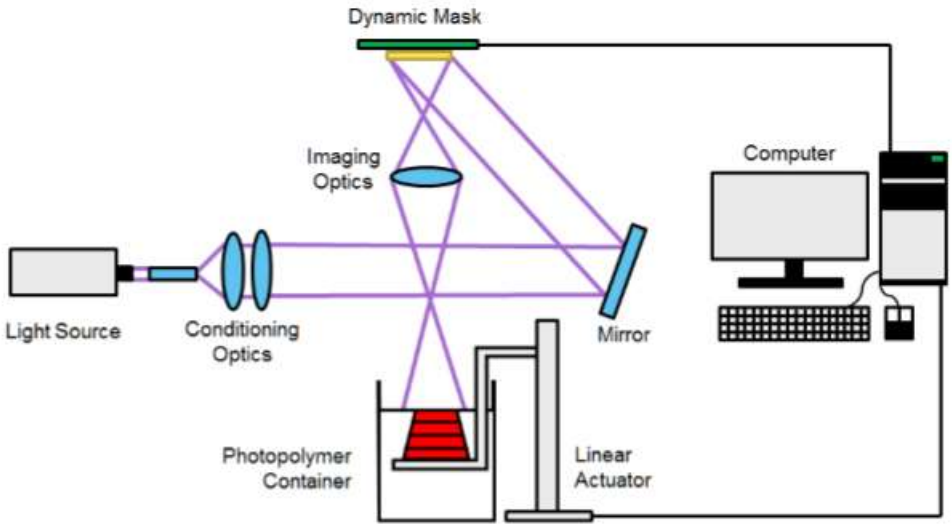

Figure 15. Schematic of a typical mask projection microstereolithography system. The purple lines represents the light traveling on the system [82]

In the setup shown in Figure 15, the light source is projected from above. Therefore, the first layer is cured on the build plate. After, the build plate lowers a desired layer height and additional resin recoats the previously cured layer to provide enough resin for the subsequent layers. The next cross-sectional layer is projected and the photocurable resin cures on top of the previous layer. This process is repeated until the final object is completed and the part is removed and post-processed if required.

2.4.2 Design Considerations in Microstereolithography

When designing a mask projection microstereolithography system, there are some requirements to be considered. The most important factors that directly affect the accuracy and speed of the 3D printing process are the light source, the dynamic mask, and the projection orientation of the system. The following paragraphs describes the available and previously used options in detail, with their advantages and disadvantages. This design analysis has led to the selection of an LCD 3D printer using a LED light source, an LCD screen as the dynamic mask and the light to be projected from bottom.

2.4.2.1 Light Source

When selecting a light source, the first important choice is to select the emission spectrum of the light source. It must include the useful wavelength of the photopolymer used on the 3D printer (match with the selected photoinitiator). Second, the intensity of the light source must be powerful enough to cure the photopolymer in a reasonable time (ideally less than 60 seconds) because this has a direct influence on the printing time.

There are three common light sources used in mask projection microstereolithography. The most commonly used light source is a lamp. It emits light in all directions, has high output intensities, and a broad spectrum. Therefore, lamps can be compatible with multiple photopolymers [83, 84]. The second light source is the LED sources. LED sources usually have longer operating lives, with lower cost, smaller sizes, and lower heat generations (more energy efficient) than lamps and lasers [85]. They usually output light in a particular wavelength, which can be tailored according to the desired photopolymer. Last, lasers should be considered. Lasers emit light at one or more wavelengths from ultraviolet, visible to infrared. However, even though lasers provide better accuracy, they are much more expensive than the other two light sources [86].

2.4.2.2 Patterned Light

The pattering of the light is the most important aspect of the mask projection microstereolithography system and is what provides the accuracy and the precision of the shape projected. There are two main dynamic masks available to digitally pattern the light source and project the light. Important aspects to be considered are the resolution, pixel pitch (the size of each pixel and the space in between), and the transmission of the dynamic mask.

The Liquid Crystal Display (LCD) screens were the first dynamic mask to be implemented in mask projection microstereolithography. LCD displays pattern light by switching pixels from opaque to transparent. This is the most inexpensive option, with the high quality of the LCD resolution (e.g. 1920x1080, and 2560x1440). The biggest disadvantage of LCD screen is that it blocks a significant amount of UV light, only transmitting 12.5% of UV light [86, 87].

The most commonly used dynamic mask is the Digital Micromirror Device (DMD) was developed due to the constraints originated from the LCD screen not transmitting UV light. This digital mask can be easily found on standard projectors. DMD discretize light over a 2D array of micromirrors, that can be individually actuated to an on and off orientation [82]. DMD offers many advantages over LCD screen, such as the possibility of using UV light sources, provides a more uniform intensity, and has greater control of exposure time. However, the DMD requires optical components to direct and scale the image produce, which can increase the price of the overall setup [21, 83, 86].

2.4.2.3 Projection orientation

When considering designs for mask projection microstereolithography, the second most important characteristic is the projection orientation. It essentially consists of selecting if the light source will be projecting from above or below the build plate. As shown if Figure 16, the two projection orientations are described. The first is a top-down orientation, where the light is projected from the top, and the second is a bottom-up orientation, where the light is projected from the bottom surface of a vat with a transparent film.

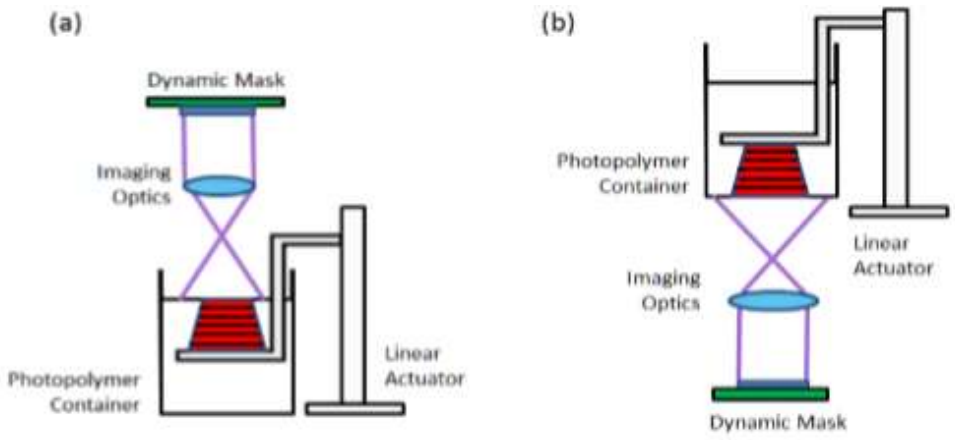

Figure 16. Diagram of the different projection orientations. a. the light source is above and b. the light source is below [82]

The most common setup in microstereolithography is when the light is projected from above. Additionally, it requires a recoat method to continue 3D printing the desired shape, which can be hard to effectively keep the layer height constant. Moreover, the recoating can significantly increase the printing time [82].

There are several advantages of bottom projection compared to top projection. Bottom projection requires less amount of photopolymer in the vat, since the build height is independent of the reservoir container [82]. Moreover, thinner layers are possible, with higher accuracy, since they are determined by the gap between the vat and the build plate. The photopolymer can also crosslink faster, because there will not be any oxygen reacting during the polymerization, increasing the reaction speed.

However, a common disadvantage of this type of orientation is that the polymer adheres in both the build plate and the thin film on the floor of the vat. Therefore, it can require about 50N to overcome this adhesion depending on the photopolymer, which can affect the printing product [83]. Researcher have been studying and developing

alternatives, such as implementing different pulling mechanisms or applying a silicon membrane on the floor of the vat [83].

3 METHODS

3.1 3D Printer

In this study, a modified LCD 3D printer (X-cube, Beijing China) shown in Figure 17, consisting of a vat of photocurable resin suspended above an LCD screen was used. This method provides excellent resolution because LCD screens can have very small pixel sizes (5.5 inches screen, 2K resolution, 2560x1440). A UV-LED (100W, 520nm CHTPON Epistar, China) was used to project the desired slices of the 3D model through the bottom of the vat. Creation Workshop software was selected to control the LCD screen, slice the CAD models and generate the G-codes that control the 3D printer. A build plate lowers into the vat of material from the top and the first layer of resin is cured on the plate. Next, the build plate rises out of the resin with the first slice of the object attached to the build plate to “peel” the object from the vat. As the object moves up, the still liquid resin flows underneath the previously cured layer. The LCD screen then projects the next layer. The uncured resin cures to the previous layer and begins to form the object (scaffold). The process is repeated, building the object layer by layer, until the model is completed. Because an entire layer of the scaffold is exposed at once, this type of 3D printing is fast, and complexity of the model does not add manufacturing time. Figure 18 shows a schematic of an LCD 3D printer.

Figure 17. Modified X-Cube LCD 3D Printer

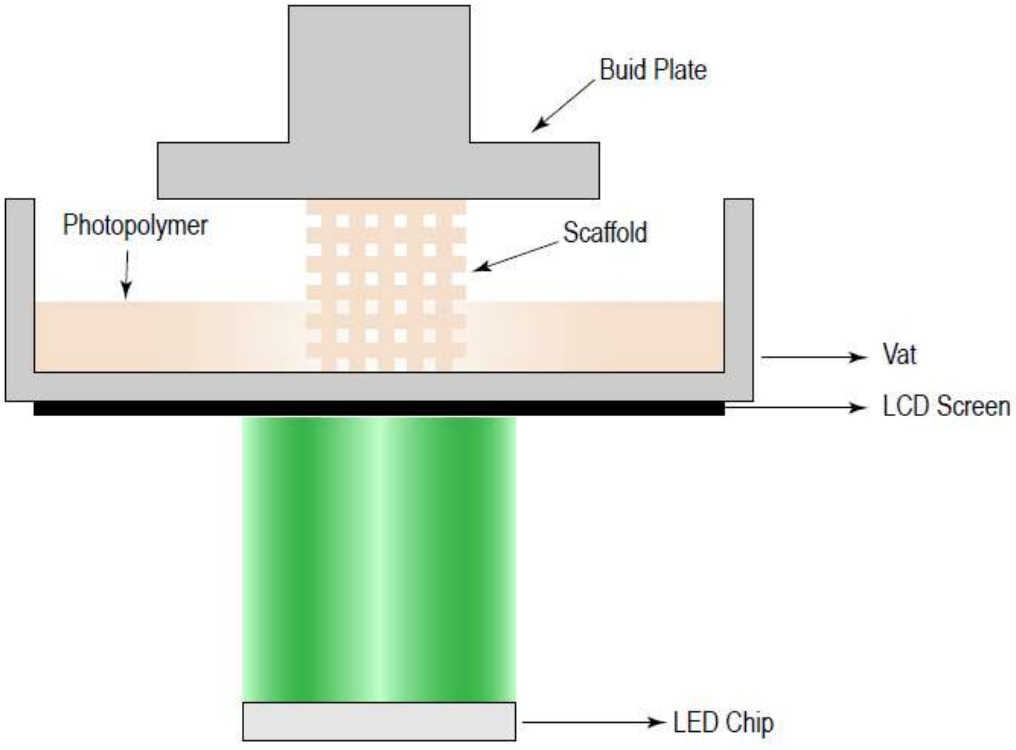

Figure 18. Schematic of an LCD 3D printer

3.2 Design modification history

The X-Cube was purchased for LCD 3D printing of PGSA. It originally had a 30W LED chip at 405nm. The first attempt to 3D print PGSA was to try to replicate the literature and use the same photoinitiator DMAP as was previously used [68]. Therefore, the wavelength of the LED chip had to be modified from 405nm to 365nm. However, that modification did not work because the LCD blocked all the UV-light source below 400nm. Next, the photoinitiator used with PGSA was replaced with a different photoinitiator that does uses wavelengths above 400nm (LCD cutoff frequency). The VA-086 was selected due to its respective spectrum with a peak wavelength at 385nm, and previous reported used with hydrogels using an SLA 3D printed laser at 405nm. However, this photoinitiator generated multiple bubbles after cured, and had a very slow curing time since its activation wavelength was below 405nm. Finally, Eosin Y was selected as the optimum photoinitiator. It is a very biocompatible photoinitiator and water soluble. However, it requires the addition of triethanolamine as a reducing agent for a faster photocrosslinking reaction. Additionally, since Eosin Y has a peak wavelength at 515nm, a 520nm 100W LED chip was purchased and implemented into the X-Cube as the final design of the printer.

The original LED chip of the 3D printer X-cube was 30W. Modifications had to be made on the printer to allow a 100W LED chip to be the light source and significantly decrease the curing time of the polymer. To accomplish this, the LED could not connect directly to the main control circuit board because it could only handle passing 30W. Modifications were made to the printer to use the signal from main board as the signal to

an externally added relay with a separate power source in order to use a much higher power LED (100W).

3.3 Synthesis/Processing of PGS and PGSA

PGS prepolymer was prepared using a condensation reaction by a procedure modified from previously published methods [26]. Three batches were made with different prepolymer curing times, but with the same acrylation procedure. These changes were made in order verify how the molecular weight of the polymer would affect the properties of the material, and to find the optimum curing time of the prepolymer for the desired application. An equimolar amount of glycerol (ThermoFisher Scientific) and sebacic acid (Sigma-Aldrich) were mixed in a 100ml round bottom flask. The reagents were stirred for approximately 4 hours (optimum value) at 140°C using an oil bath. For Batch 1 the prepolymer was cured for 3 hours, Batch 2 for 3.5 hours 4 hours for Batch 3. A vacuum of 25mbar was applied during the reaction to remove moisture and drive the reaction to completion.

For acrylation, the PGS prepolymer was dissolved in dichloromethane (DCM, ThermoFisher Scientific). 0.1wt% of 4-(dimethylamino) pyridine (Sigma-Aldrich) was added into the mixture. An equimolar amount of triethylamine (TEA- Sigma-Aldrich) and Acryloyl Chloride (Sigma-Aldrich) were added dropwise simultaneously into the stirred solution. The reaction flask was kept at room temperature for 10 minutes. Ethyl acetate (Sigma-Aldrich) was added into the mixture and the flask was placed on the freezer for 3 hours to cool. The solution was removed from the freezer and the mixture was vacuum filtered immediately to remove the TEA salt produced during the reaction. Ethyl acetate was then removed using a rotary evaporator under vacuum with a 50°C

water bath to leave a viscous liquid of PGSA. This procedure was slightly modified from previously reported acylation methods of PGS prepolymer [33, 66]. The photoinitiator Eosin Y was used as a photoinitiator with triethanolamine as a reducing agent. 0.75 vol% of triethanolamine was mixed with 0.1mM of Eosin Y, with an additional 0.1 vol% of ethanol. Figure 19 illustrates a schematic of the synthesis process of PGSA and Figure 20 shows the reaction schematic of PGS prepolymer and PGSA.

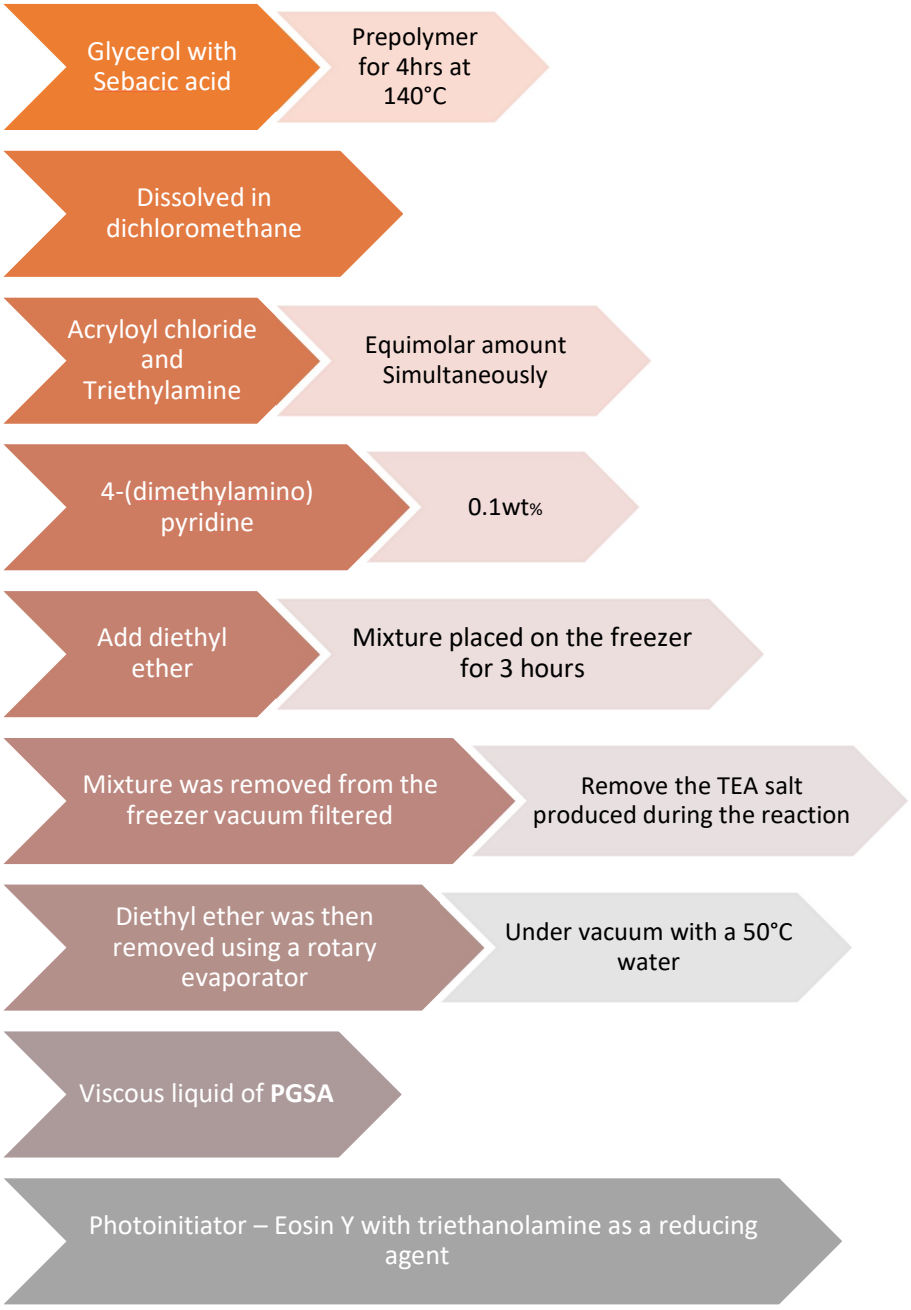

Figure 19. Schematic of the synthesis process of PGSA

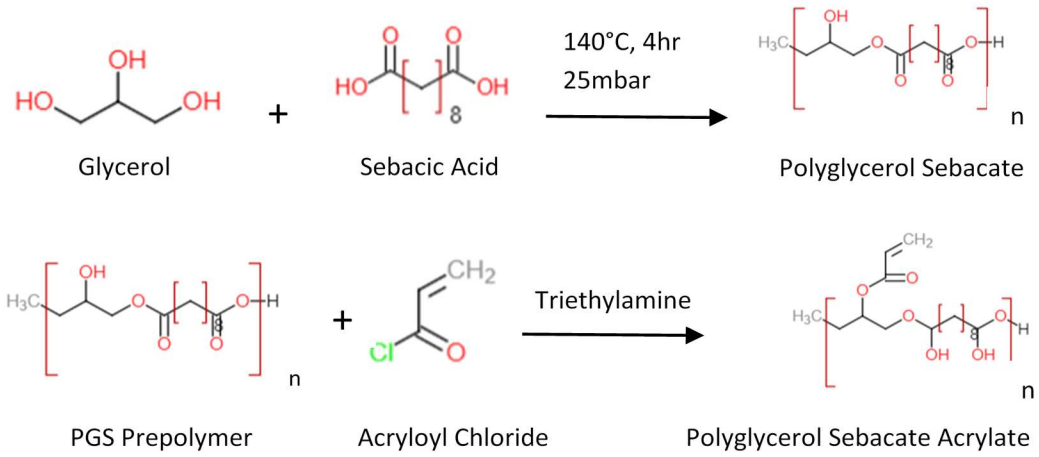

Figure 20. Reaction schematic for PGS prepolymer and Polyglycerol Sebacate Acrylate

3.4 Polymer characterization

3.4.1 Polymer characterization via FTIR

Fourier Transform Infrared Spectroscopy (FTIR) analysis was performed on a Nicolet 380 (Thermo-Scientific, USA) to characterize the prepolymer and photocured PGSA (LCD 3D printer). The tests were performed on the following machine shown in Figure 21.

Figure 21. Machined used to perform FTIR tests

3.4.2 Rheological measurement

The viscosity is a major material parameter in many processes [88]. In LCD 3D printing, the viscosity of the resin is critical for a successful print and characterizing the rheological properties of the polymer can be used to find the optimum printing parameters. Moreover, after the desired shape is cured into the build plate, the remainder resin needs to slide underneath the build pate before the next layer begins to cure. Most rheological tests are performed by keeping the bottom plate fixed while the top plate either rotates or oscillates [89]. By using a rheometer, multiple characteristics of a polymer can be determined, such as its shear viscosity (Pas), storage and loss modulus (Pa), phase angle (δ), angular frequency (rad/s), and time dependent properties such as stress relaxation modulus, creep, and recoverable compliance.

Rotational and oscillatory rheological tests were performed on the prepared PGSA samples using an AR2000 stress-controlled rheometer (TA Instruments, USA) shown in

Figure 22. The rheological measurements were made using a parallel plate configuration. The viscosity of the different batches of PGSA were determined by measuring the slope of the shear rate versus shear stress plot. The rotational test on the three batches were conducted under continuous flow (0.0–50.0 s^{-1}) with an equilibration duration time of two minutes and the gap distance was set to 1500 microns for the entire test. A similar procedure was performed in a previous study [68]. Additionally, two commonly used 3D printing resins were used to for direct comparison (Makerjuice [90] and Formlabs [91]) following the same procedure. Figure 23 shows the rheological test being performed with PGSA.

Figure 22. AR2000 Rheometer used to perform viscosity tests

Oscillatory tests were performed on the viscoelastic polymer. A frequency sweep was performed at a constant temperature (25°C), and angular frequency varied from 0 to 100 rad/s. Time dependent properties and crossover point of the storage modulus (G', which is equal to the deformation of energy saved by the biomaterial) and the loss modulus (G", which is how much of deformation energy that was used by the biomaterial) were determined [89]. A strain sweep was also performed to provide a deeper understanding of the material rigidity and strength [92]. The sample was subjected to a small amplitude oscillatory test. The storage G′ and loss G″ moduli were monitored under 0.5% strain, constant frequency of 1 Hz, and at 25 °C.

Figure 23. Rheological test being performed at a PGSA sample

3.5 Swelling testing

Swelling by hydration was measured by the mass differential after the PGSA samples were submerged into a PBS media for a total of 72 hours. The PGSA samples used were the same as used for biocompatibility tests, where they were 3D printed with 10mm diameter and 3mm thickness. The PGSA samples were weighted (W_0) before the swelling test. PGSA samples were submerged in PBS media for 24 hours until peak swelling and was kept for an additional 48 hours until it reached equilibrium. Then, the fully swelled samples were weighed and measured again (W_1) following the same procedure. The swelling ratio was calculated based on the weight change using the following equation:

$$SR = \frac{W_1 - W_0}{W_0} x100\%$$

3.6 Mechanical testing

For tensile testing, four samples from each batch of PGSA samples were prepared on LCD 3D Printer as dog bone shaped specimens (~ 3mm height, overall length of 24mm, and a narrowed section that was 5.5mm long and 4mm wide) [26] as shown in Figure 24. Samples were loaded into textured grips on an MTS Insight electromechanical testing system as shown in Figure 25 (MTS Insight, USA, 250N loadcell), and tested with a 0.01N pre-load a rate of 5mmmin^{-1} until failure. The texture grips were attached into the fabric clamps fixture (glued sand paper into the fixture), which are shown in Figure 26, which were essential for the samples not to slip or cause any damage during the tests. All the samples were soaked in a PBS media for approximately 24 hours before the testing was performed.

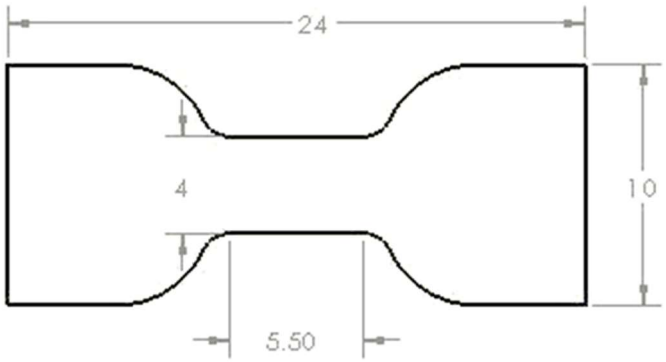

Figure 24. Drawing of the tensile specimen with dimensions in mm used for mechanical characterization

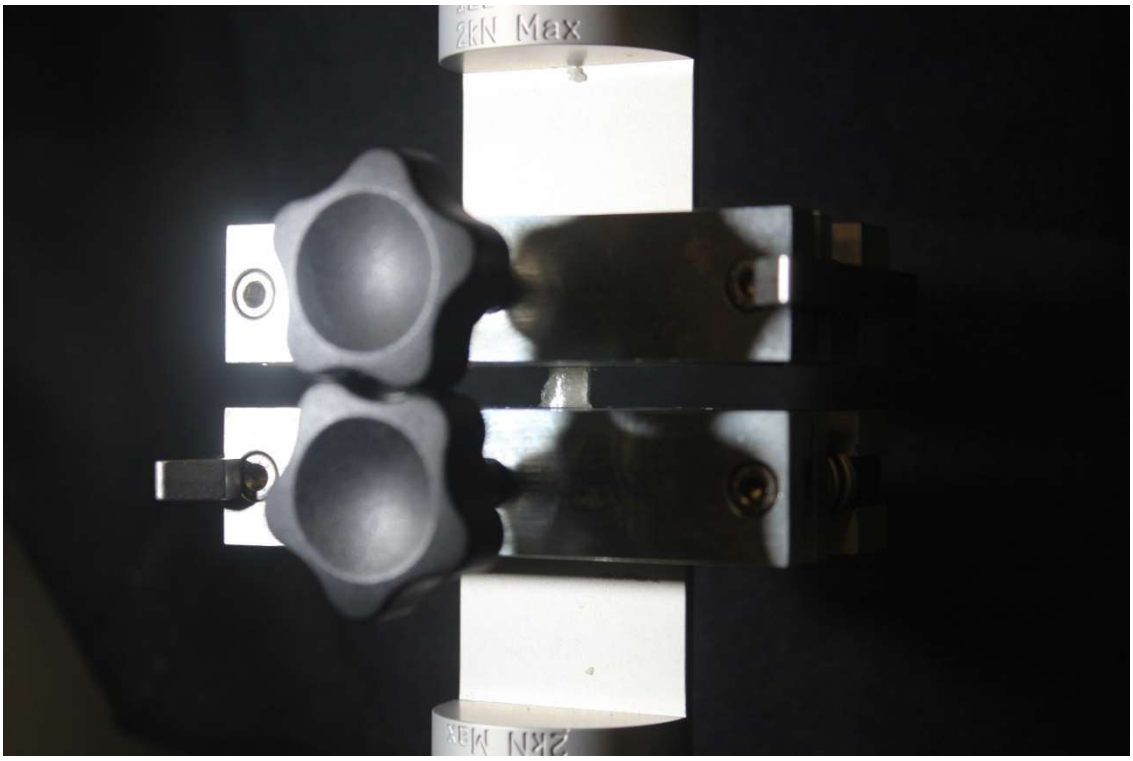

Figure 25. Tensile test setup at MTS Insight

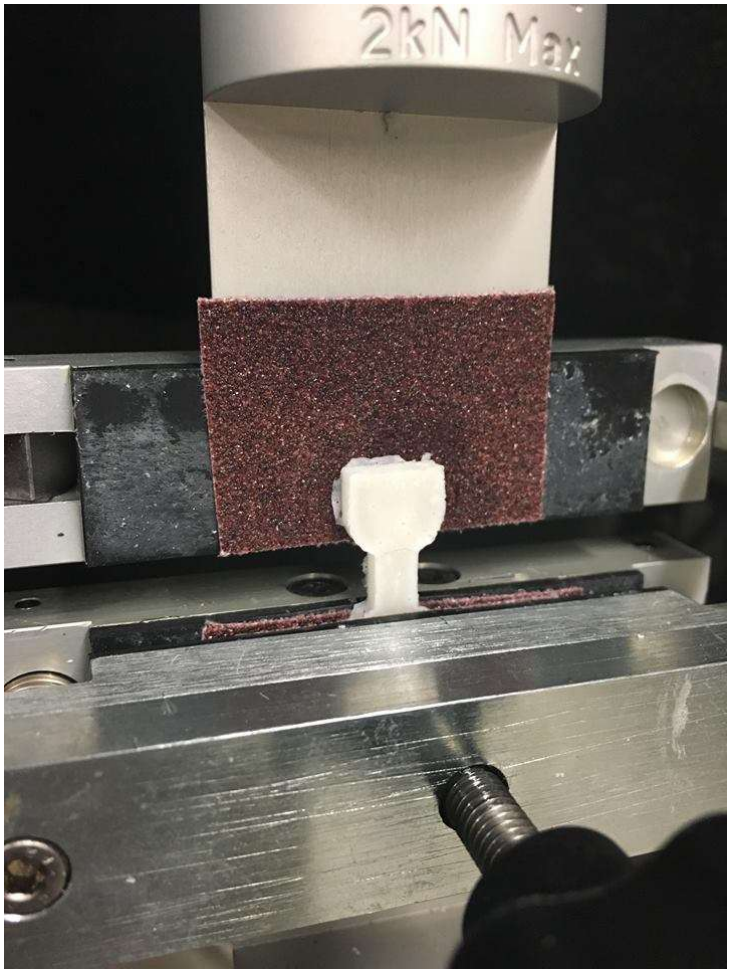

Figure 26. Representative test setup for the tensile test showing modified texture grips

Displacement and force data were recorded during loading, and then post processed using a custom written analysis code (MATLAB, MathWorks) to determine sample stresses (forces divided by cross-sectional areas), ultimate stresses (the highest stress attained), failure strains (strain values where failure stresses were achieved), and elastic moduli (calculated from the slopes from 40% to 50% of failure strains) [68] . Additionally, the crosslinking density (n) was calculated according to the theory of rubber elasticity using the following equation [26]:

$$n = \frac{E_0}{3RT}$$

Where E_0 is Young's modulus, R is the universal gas constant, T is the absolute temperature (K), and n represents the number of active network chain segments per unit volume (mol m^{-3}) [26].

3.7 Biocompatibility

Biocompatibility tests were performed to verify the cytocompatibility of the polymer and to prove that no harmful substances remained behind after fabrication and printing of the PGSA. Before testing, hydrophilic crystals remaining in the liquid polymer were removed by washing with DI water. After several minutes, the water and the material were visually separated since PGSA is hydrophobic, and the DI water could be removed. Water and PGSA were separated using centrifugation and the water was discarded. On one occasion, water remained after centrifugation but separated from the PGSA overnight at 4°C.

3D printed, biocompatible growth chambers with dimensions of 10mm diameter and 3mm thick were created with a hollow square trough with dimensions of 5mm long and 0.25mm thick to help trap cells and enable a longer period of time for adhesion. The chambers are shown in Figure 27. Chinese Hamster Ovary (CHO) Cells were cultured in Dulbecco's Modified Eagles Medium (DMEM) without phenol red, with 10% fetal bovine serum and 1% penicillin-streptomycin (10K index units) at 37°C under a humidified atmosphere with 5% CO_2. For cell seeding, 3D printed PGSA scaffolds were sterilized by incubation in PBS with antibiotic for three days, with daily rinses in PBS-antibiotic of 20 times the volume of the chamber. Additionally, one rinse in 4 mL of media was made before plating cells. As an initial test of cell adhesion and viability, CHO cells were placed onto a 3D printed chamber from each batch and incubated

overnight in PBS with antibiotic. PGSA chambers were kept in small 35mm diameter culture dishes. Images of cells were acquired using an Olympus FV1200 confocal system with an IX81 inverted microscope showing that the cell adhered within the PGSA chamber and also to the bottom of the culture dish. Cells adhered to the bottom of the dish were imaged using phase contrast with a Face contrast inverted microscope Zeiss Axiovert S100TV. Cells adhered inside the chambers were imaged with a fluorescent marker, GPI-td-tomato, which is made and secreted to the plasma membrane of live cells. GPI-td-tomato is a lipid anchored surface protein with excitation-emission spectra similar to rhodamine.

Figure 27. 3D Printed chambers for biocompatibility tests

3.8 3D Printing

The customized LCD 3D printer was used to create all the mechanical, swelling and biocompatibility samples for testing purposes. The output resolution was set to 50 microns, with a slice thickness of 0.05mm. The exposure time for was set to approximately one minute for Batch 3, one minute and a half for Batch 2, and two minutes for Batch 1. This value can also be tailored according to the desired stuffiness of the sample (decreasing curing time directly decreases the stuffiness of the sample), and

by the amount of photoinitiator in each sample. Moreover, since Batch 3 had a higher prepolymer curing time and therefore higher molecular weight, it required a lower curing time when compared to the other batches. For testing purposes, the amount of photoinitiator was kept constant as previously mentioned in the synthesis and processing section of PGSA.

Four solid dog-bone structures were 3D printed for tensile tests for each batch. Representative samples from Batch 3 are shown in Figure 28. Four biocompatibility chambers were also 3D Printed and used for the swelling tests.

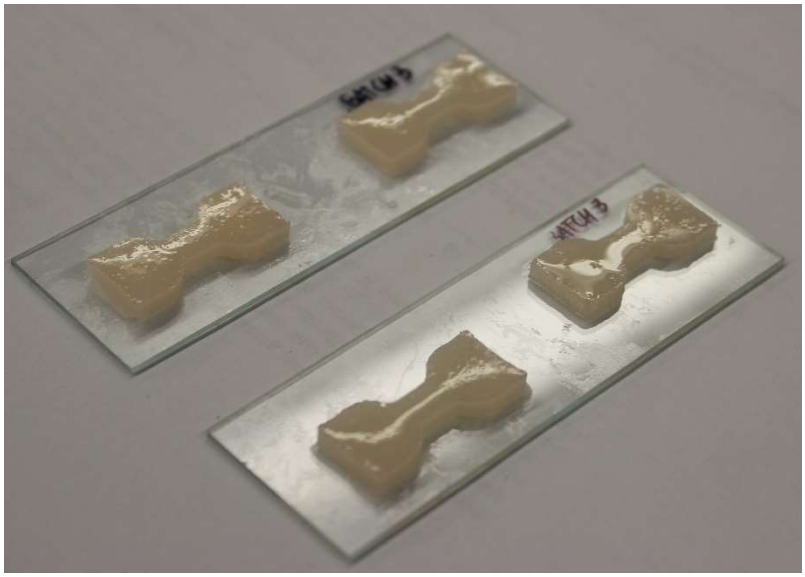

Figure 28. The four tensile samples used for tensile tests from batch 3

4 RESULTS

4.1 Polymer characterization

Fourier Transform Infrared Spectroscopy (FTIR) analysis was used to characterize the chemical structure of the material. PGS prepolymer, uncured PGSA and LCD 3D printed PGSA samples were characterized using methods previously published [26, 33]. Based on Wang's study [26], the prepolymer results presented comparable signature bands with an intense stretch of the C=0 at 1696 cm^{-1} that confirms the formation of ester linkages as shown in Figure 29. Moreover, it also presented an intense OH stretch at 3500-3200 cm^{-1} indicating that the hydroxyl groups are hydrogen bonded [26].

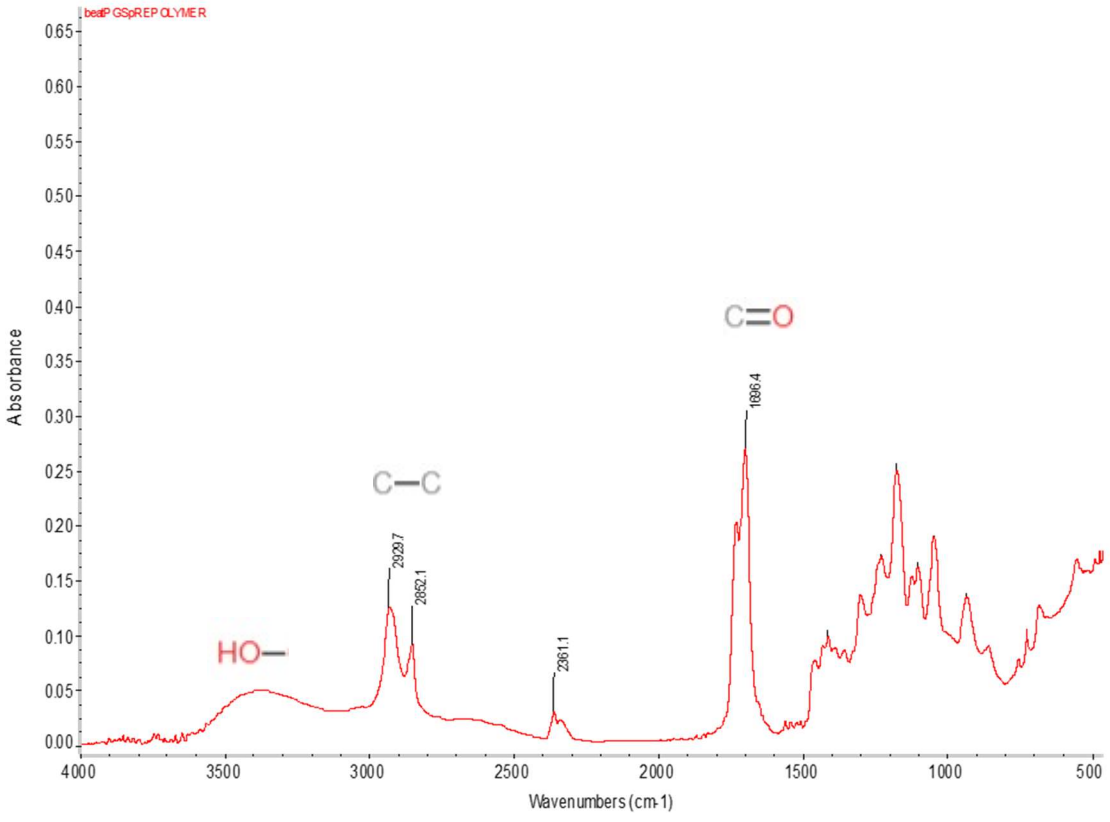

Figure 29. Representative FTIR Spectrum of PGS Prepolymer

For the photocured PGSA material, Nijst's study was used to verify our findings [33]. The goal was to confirm the crosslinking reaction of the polymer. The addition of acrylate groups was confirmed with the appearance of an absorption band that represents the CH stretching of the second alkyl group at 1375cm^{-1} [33].The result for the acrylated PGSA is shown in Figure 30. The characteristic absorption bands of hydroxyl (3500-3200 cm^{-1}) and ester (1800-1600 cm^{-1}) groups in the polymer backbone changed after the polymer was photocured. The formation of the polymer network after photocuring PGSA was confirmed by the increase of the 1731.4cm^{-1}, and reduction of the absorption bands of hydroxyl (3500-3200 cm^{-1}) and the significant reduction of the peak at 1375 cm^{-1}, known to be associated with acrylate groups [33]. The results of the photocured PGSA are shown on Figure 31.

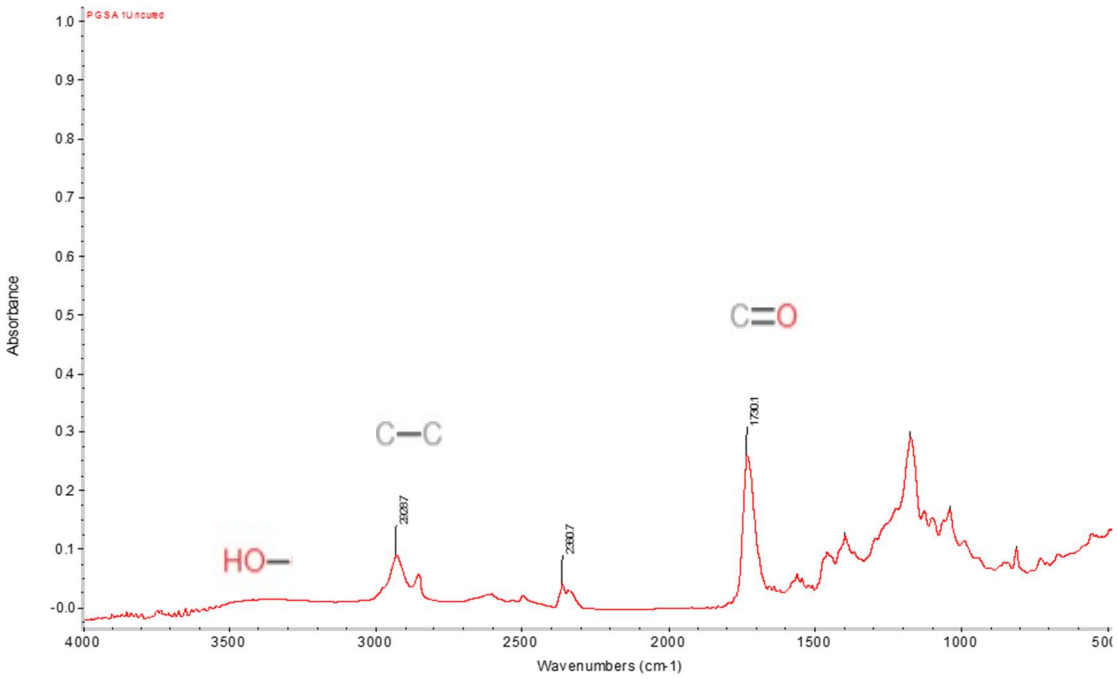

Figure 30. Representative FTIR Spectrum of Uncured PGSA

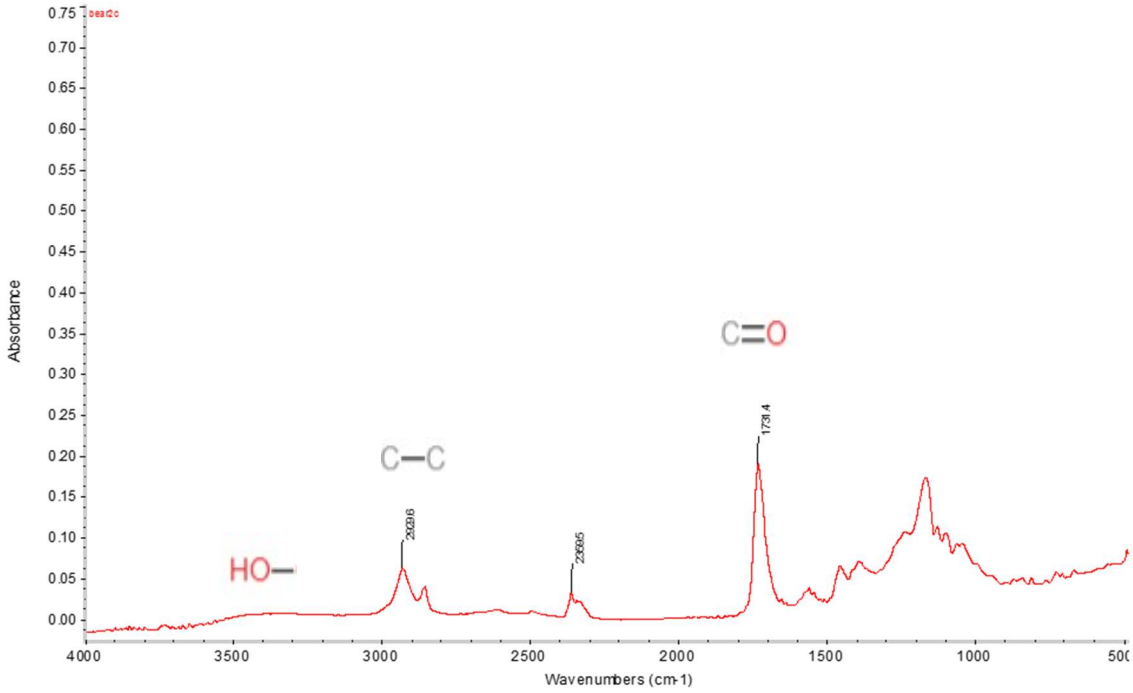

Figure 31. Representative FTIR spectrum of a cured PGSA using LCD 3D printer

4.2 Rheological Results

The viscosity of the photocurable resin is essential for SLA/LCD 3D printer. Viscosity for two commonly used resins, MakerJuice [90] (typically used to create solid materials) and FormLabs [91] (typically used to create flexible materials) were selected for comparison with the viscosities of PGSA before crosslinking, to ensure printability. Also tested, the three different batches of PGSA manufactured on separate occasions to test repeatability and curing times. PGSA Batch 1 was 3 weeks old, with PGSA Batch 2 being 5 days old, and PGSA Batch 3 was 1 day old. All the tests were performed at room temperature (25°C).

The average viscosity of PGSA Batch 1 was found to be 3.57±0.17 Pa.s, PGSA Batch 2 was 3.62±0.16 Pa.s, and PGSA Batch 3 was 15.62±0.90 Pa.s, as shown on Table 1. The results obtained from Batch 1 and 2 were slightly above the ranges of the

commonly used resin FormLabs, and Batch 3 had a significant increase in viscosity, due to its longer curing time (higher molecular weight that causes the polymer to become much more viscous). The FormLabs resin average viscosity was found to be 2.19±0.04 Pa.s and the average MakerJuice viscosity was found to be 0.12±0.01 Pa.s. Although slightly higher than common 3D printing resins, the viscosity of PGSA was showed to be consist between the first two batches of PGSA polymer manufactured. However, all the PGSA samples are within the acceptable range of viscosities used in SLA/DLP printers (less than 20Pa.s). Figure 32 shows the plot of shear stress versus shear rate of all the materials tested and the changes in viscosity as the shear rate increases of the same materials is shown on Figure 33.

Table 1. Average Viscosity of commonly used 3D Printing resins and PGSA from different batches

Material	Average Viscosity (Pa.s)
Formlabs	2.19±0.04
Makerjuice	0.12±0.01
PGSA1	3.57±0.17
PGSA2	3.62±0.16
PGSA3	15.62±0.90

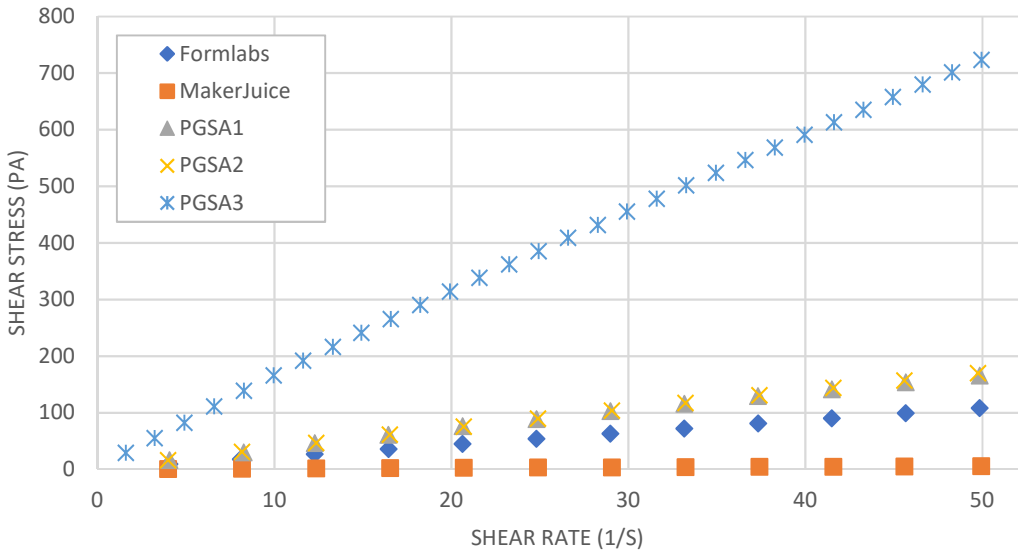

Figure 32. Shear stress-shear rate plots of different materials.

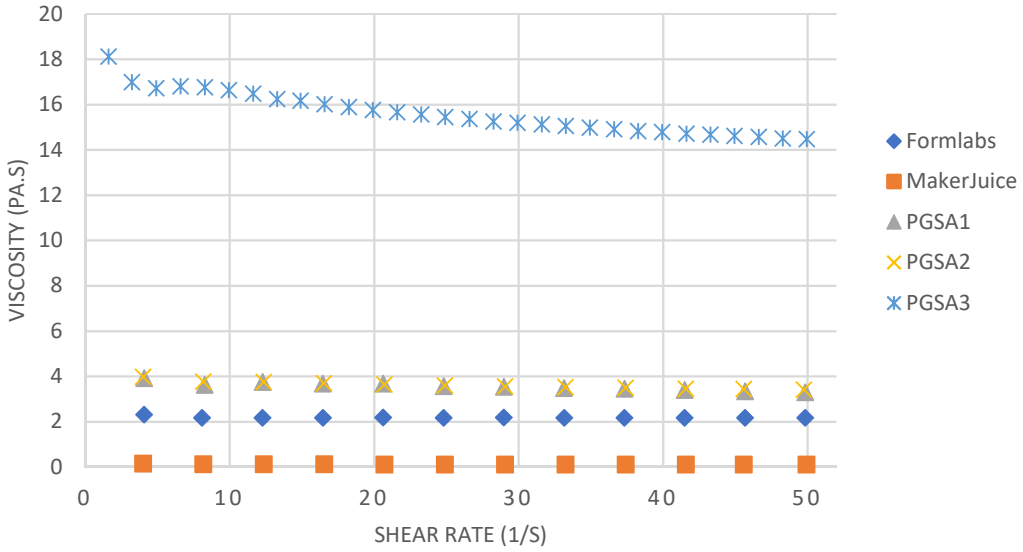

Figure 33. Shear rate plots of different materials

Next, an oscillatory frequency sweep test was performed on the three batches of PGSA and presented on Figure 34, Figure 35 and Figure 36 respectively. When the PGSA presents a higher G" than G' it demonstrates a viscous or liquid behavior (also an

uncross-linked behavior). On the Batches 1 and 2 the material behaved slightly different, showing a higher G" than G' until the material reached the cross-over point at the intersection of the G’ and G’’ (at approximately at 40 rad/s on batch 1 and 80 rad/s on batch 2), where the gel-solid transition temperature was achieved by shifting the molecular weight distribution of the polymer, which it was not visible for the polymer on Batch 3.

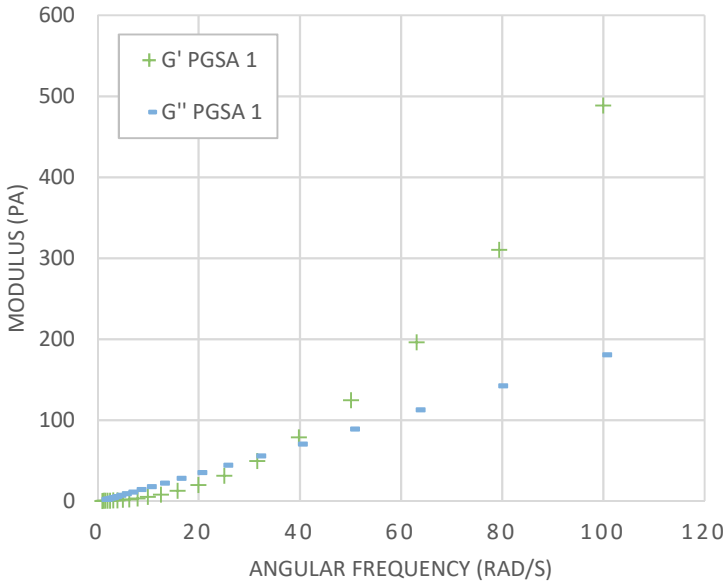

Figure 34. Frequency Sweep of PGSA from Batch 1

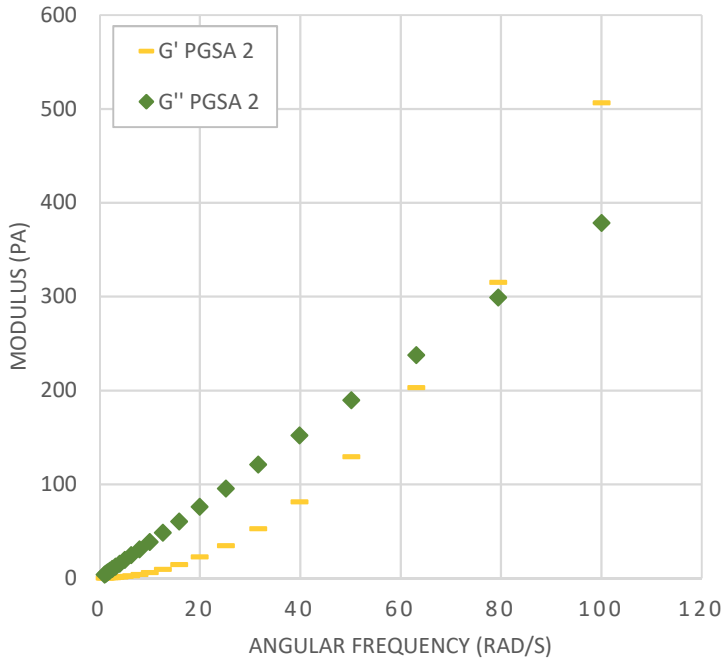

Figure 35. Frequency Sweep of PGSA from Batch 2

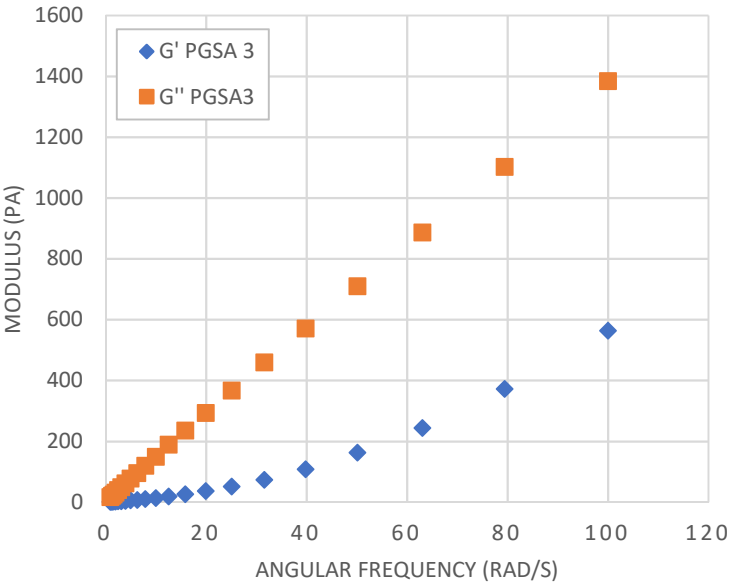

Figure 36. Frequency Sweep of PGSA from Batch 3

Finally, strain sweep tests were performed to comprehend the material rigidity and strength of PGSA. Theoretically, as the applied stress increases it causes an ultimate

disturbance of the polymer structure (yield) causing the phase angles to rise and the rigidity to decrease [92]. The test results of each batch of PGSA are shown on Figure 37, Figure 38 and Figure 39 respectively. They did not demonstrate any significant damage of the polymer, as there was no drastic decrease on any of the modulus.

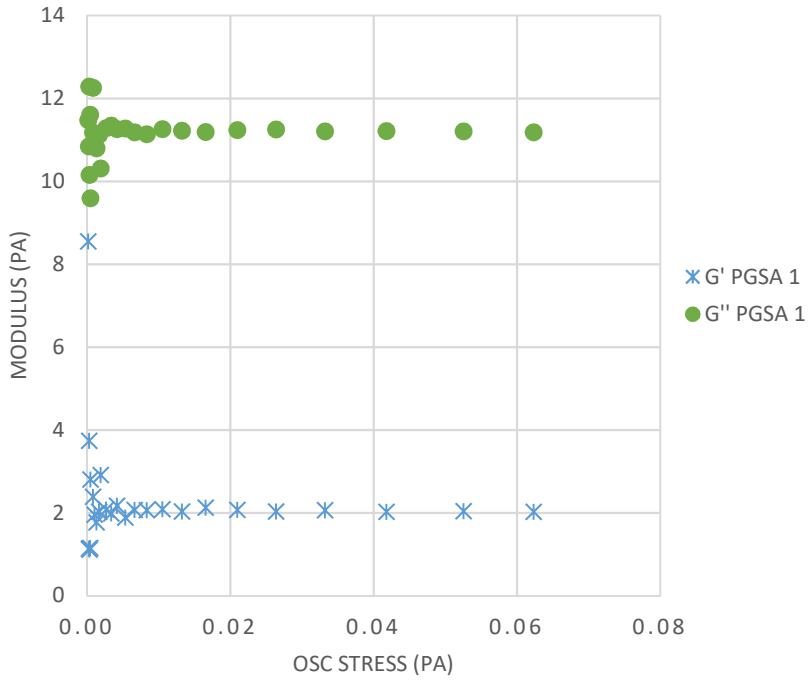

Figure 37. Strain Sweep results of PGSA from Batch 1

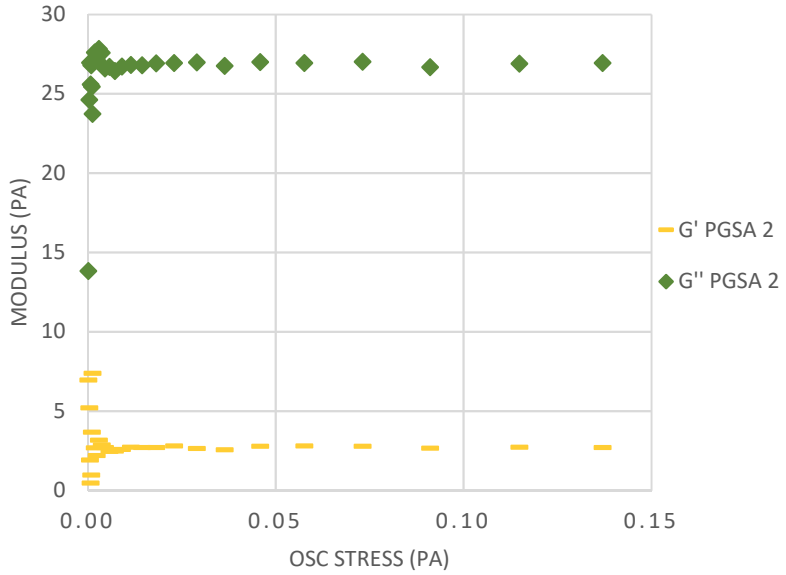

Figure 38. Strain Sweep results of PGSA from Batch 2

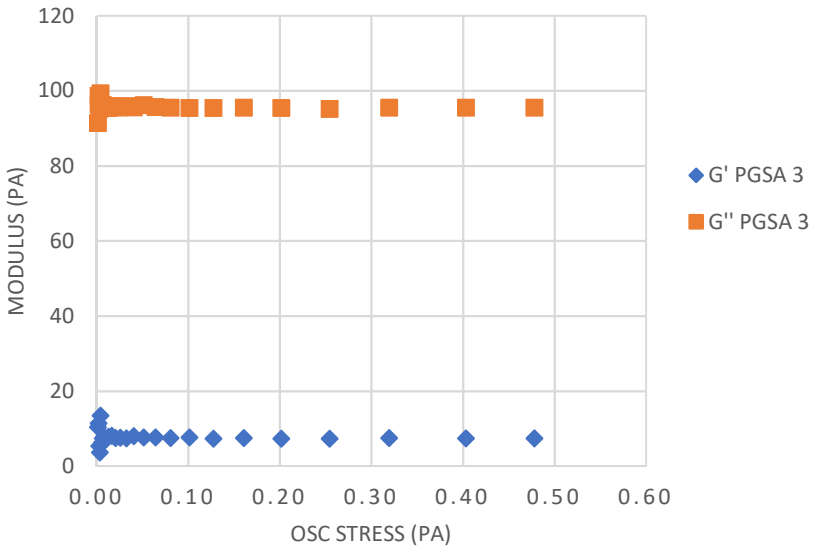

Figure 39. Strain Sweep results of PGSA from Batch 3

4.3 Swelling Results

The polymer was found to be insoluble in water. The degree of swelling in PBS media for 24 hours of the polymer was found to be 6.45% for Batch 1, 12.94% for Batch 2 and 13.11% for Batch 3. The sample from Batch 1 and 3 did not present any visual cracks due to the swelling, however, the samples in Batch 2 were significantly damaged by the stress caused during the swelling test. During further tensile tests, those cracks were also visible, and it might have affected the end results of the tests. However, even though Batch 3 presented the maximum swelling percentage, the sample was the least impacted by the swelling rate on the mechanical tests.

The test continued with the same media for an extra 48 hours and the samples were soaked for a total of 72 hours. After 72 hours, the degree of swelling of the polymer were found to be -1.43% for Batch 1, 2.36% for Batch 2 and 9.22% for Batch 3. These results show that the polymer likely started degrading in solution for Batch 1. Also, it can be concluded that after 72 hours, the sample that was more constant was the sample from Batch 3, showing that the changes in swelling ratio affected that sample less than the other two samples.

4.4 Mechanical Properties

Four 3D printed dogbone samples from different batches of PGSA were soaked for approximately 24 hours prior testing. While the samples were wetted before testing and showed some swelling, most of the samples from Batch 2 had visual cracks shown in Figure 40, which might have significantly affected the results obtained for that batch. Also, Batch 1 presented significant swelling, while Batch 3 did not present significant swelling or changes compared to the other two batches. Young's modulus was

determined from the slope of the linear portion of the plot (<15% strain) and varied from ~0.0039 to 2.073MPa depending on the batch of the PGSA. The ultimate tensile stress from the three batches varied from ~0.0068 to 0.315MPa. The maximum elongation varied from ~11.6 to 91.1%. A representative graph of each batch is shown in Figure 41.

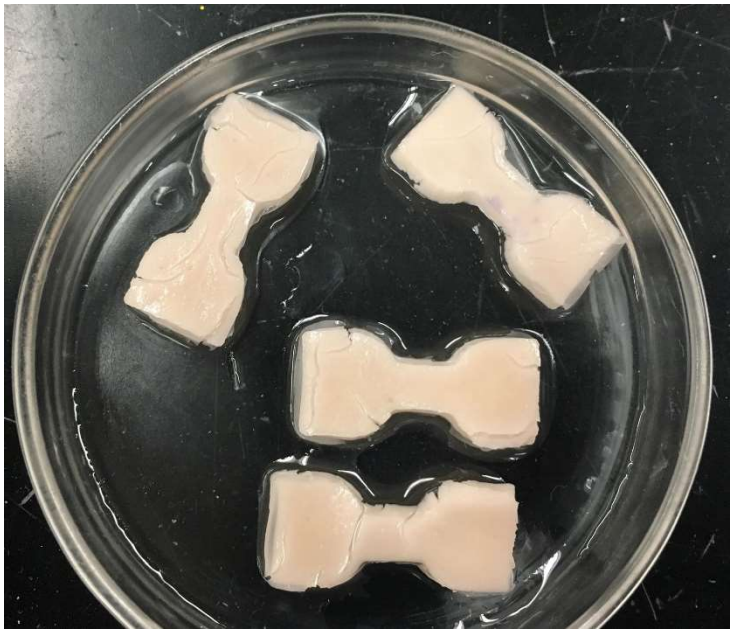

Figure 40. Tensile samples from batch 2 with visual cracks noticeable

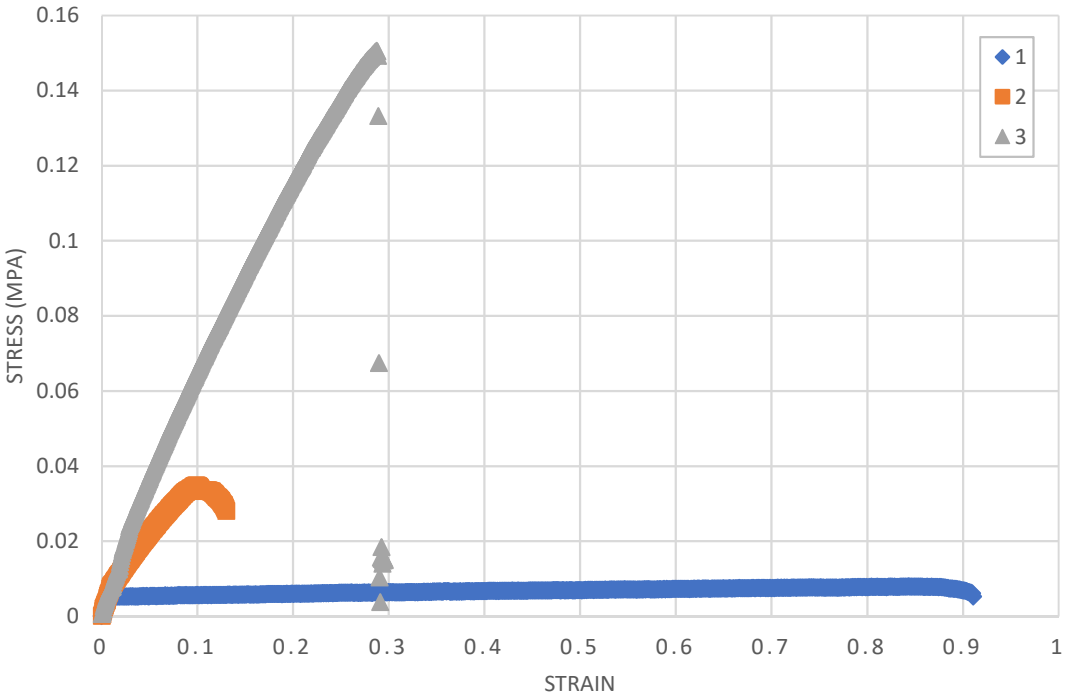

Figure 41. Representative Stress vs Strain Curves of batches 1, 2 and 3 of PGSA

The significant changes in stiffness and ultimate stress of the polymer is directly proportional to the curing time of the prepolymer. Typically, PGS shows elastomeric properties and this was clearly shown in the Batch 1 results[26], since this batch had the lowest curing times of the three batches. However, due to the longer curing time, Batch 3 has a higher molecular weight and is much stiffer than the other batches. The average Young's Modulus of Elasticity, Ultimate tensile stress and maximum elongation of the three batches are presented on Table 2 and compared on Figure 42 and Figure 43.

Table 2. Average mechanical properties of the three batches of PGSA

	Max Tensile Stress (MPa)	Young Modulus (MPa)	Max Strain (%)
1	0.0074±0.001	0.0039±0	87.60±3.5
2	0.0416±0.007	0.3893±0.070	14.03±1.0
3	0.1621±0.059	1.2749±0.464	17.14±2.3

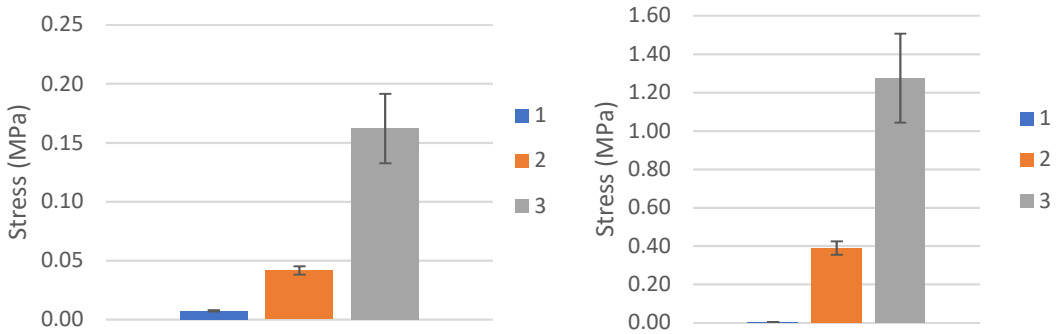

Figure 42. Direct comparison of the Maximum Tensile Stress on the three batches of PGSA (left). Direct comparison of the Young's Modulus of Elasticity of the three batches of PGSA (right)

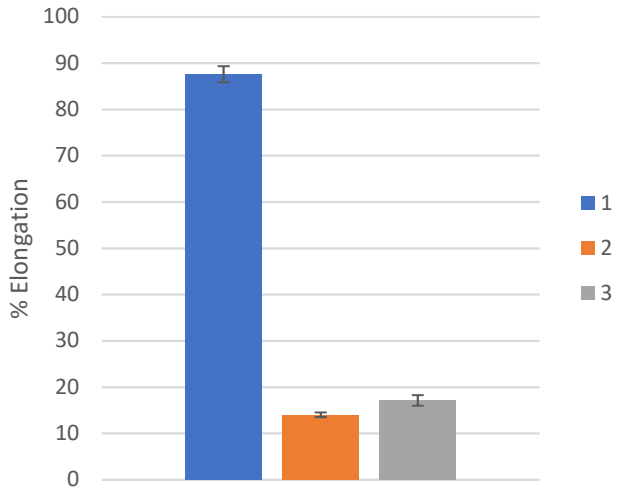

Figure 43. Direct comparison of the maximum strain of the three batches of PGSA

As shown in Table 2 and on the following figures, as a characteristic of an elastomer, Batch 1 has very low ultimate tensile stresses compared to the other two batches, but it presents a much higher percent of elongation. Because Batch 2 samples showed significant visible cracking, it is hard to know if the results were very accurate.

However, because the curing time of Batch 2 was in between of Batch 1 and 3, its mechanical properties were also in the middle range of these two. The tensile samples form Batch 3 after soaking are shown in Figure 44. Batch 3 is the stiffest batch, with higher ultimate stress and Young's modulus of elasticity but lower percent elongation. Therefore, this shows that by controlling the prepolymer curing time, the mechanical, swelling and rheological properties of the material can be tailored according to the desired application.

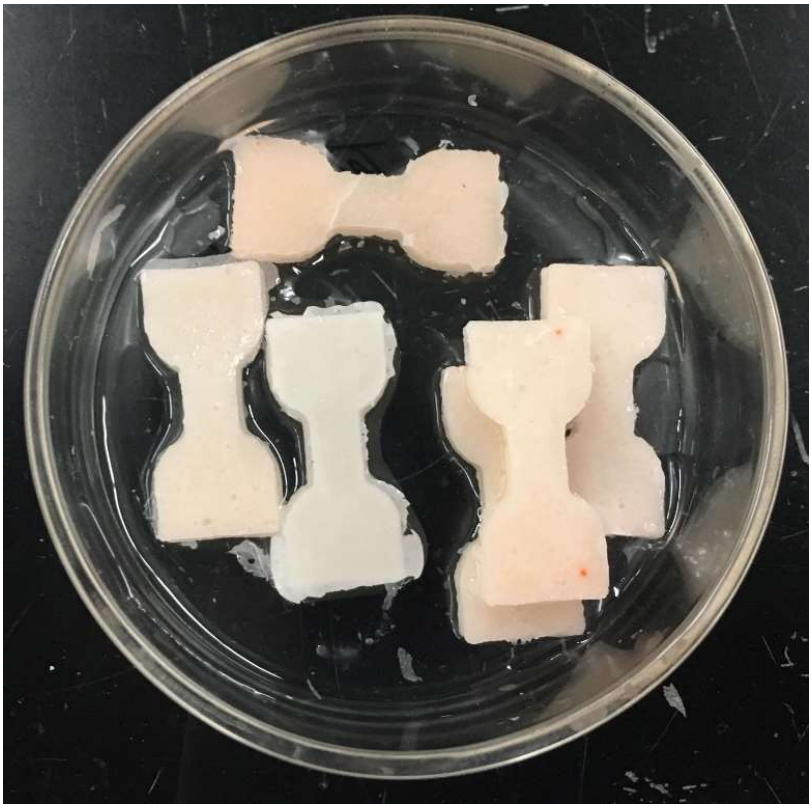

Figure 44. 3D printed tensile tests samples wet from Batch 3

Because Batch 3 showed the lowest amount of swelling in culture media environment, comparisons between a dry and wet environment before tensile tests were performed and the results are shown below. Table 3 describes the average of the mechanical properties of the Batch 3 in a dry and wet environment before the tensile test

was performed. Moreover, Figure 45, Figure 46, and Figure 47 describes the direct comparison of these properties.

Table 3. Average mechanical properties of 3D printed samples from batch 3 at a dry and wet environment prior to testing

	Max Tensile Stress (MPa)	Young Modulus (MPa)	Max Strain (%)
Dry	0.2776±0.029	1.7336±0.210	22.13±3.7
Wet	0.1621±0.059	1.2749±0.464	17.14±2.3

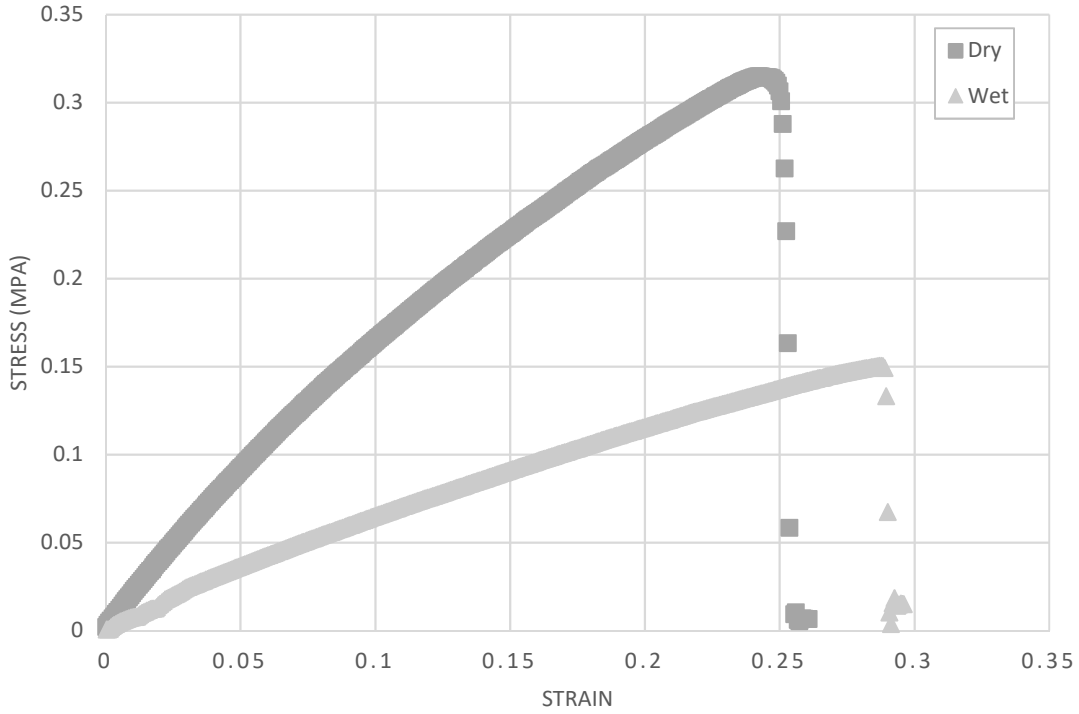

Figure 45. Representative Stress vs Strain curves of the 3D printed tensile samples from batch 3 at a dry and wet environment prior to testing

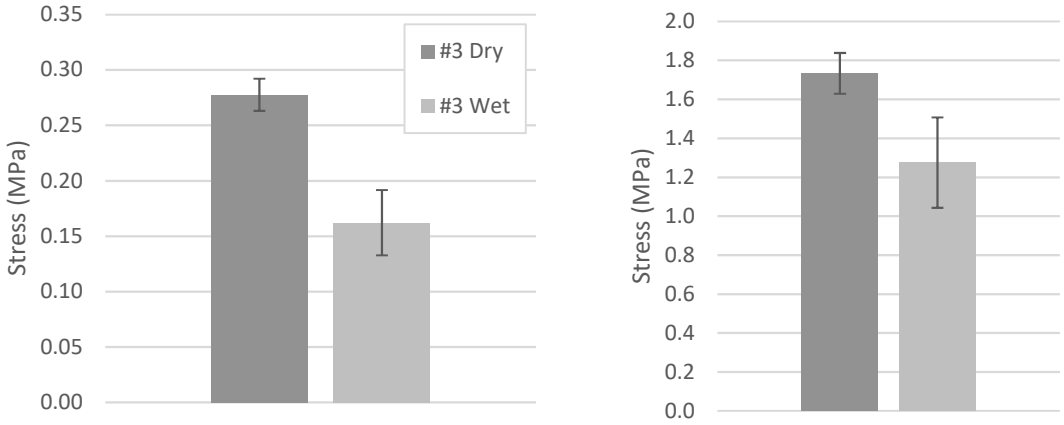

Figure 46. Direct comparison of the Maximum Tensile Stress of the 3D Printed tensile samples on a dry and wet environment prior to the test (left). Direct comparison of the Young's Modulus of Elasticity of the 3D Printed tensile samples on a dry and wet environment

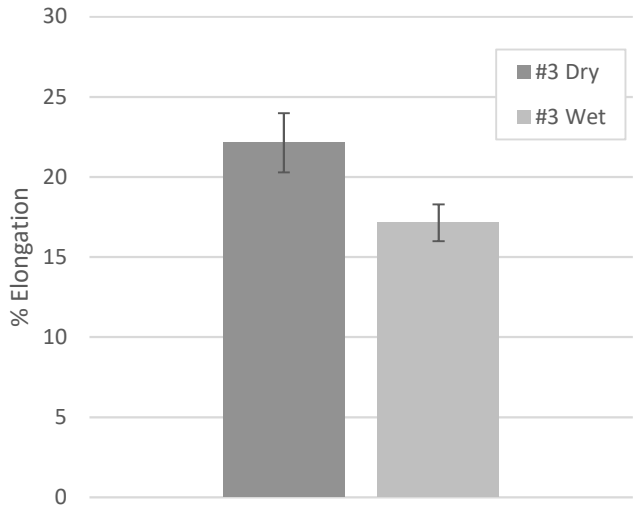

Figure 47. Direct comparison of the Percentage of elongation of the samples form batch 3 from a dry and wet environment

The mechanical properties of PGSA from Batch 3 after a dry and wet environment some significant changes. An example of a tensile sample after failure is shown in Figure 487. The wet ultimate tensile stress decreased by 41.6%, the Young's modulus of Elasticity decreased by 26.5% and the maximum percentage of elongation

decreased by 22.5% when compared to the dry samples. Therefore, it can be concluded that the Batch 3 is the best batch for biocompatibility tests, since its mechanical properties did not significantly change after being soaked for approximately 24 hours, and it did not present any visual crack on the samples like the other batches.

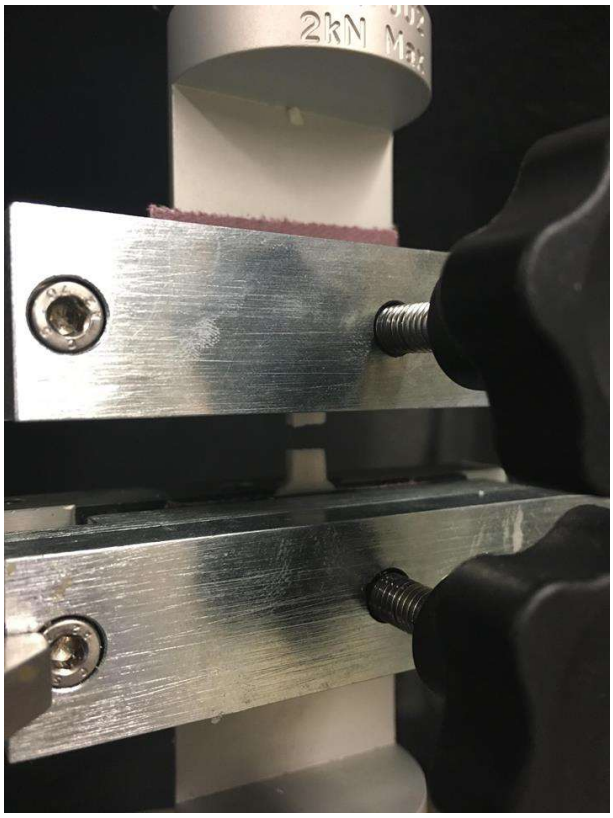

Figure 48. Representative tensile failure of a PGSA sample from Batch 3

The crosslinking density of the different batches was expressed by n (moles of active network chains per unit volume), which is 0.53 ± 0.00 mol/m^3 for Batch 1, 52.73 ± 9.48 mol/m^3 for Batch 2 and 172.70 ± 62.85 mol/m^3 for Batch 3, and it was calculated from the following equation [26]:

$$n = \frac{E_0}{3RT}$$

Where E_0 is Young's modulus, R is the universal gas constant, T is the absolute temperature. Again, these shows how the crosslinking density increase with curing time and increase in curing temperature [32]. The increase in crosslink density also led to a notable increase in tensile strength and modulus, as well as hydrophilicity [74].

4.5 Biocompatibility

The first tests were performed on biocompatibility chambers from Batches 1 and 2. Several cells were alive, and that they adhere to the PGSA chamber, however the cells did not group together. Figure 49 shows on the bottom of the culture dish of the PGSA from Batch 1, which most are spread and healthy, indicating that the polymer did not produce any toxic elements into the media. Figure 50 shows the same image from the top of the chamber using a fluorescence inverted microscope with GIS tdTomato. Figure 51 shows the cell on top of the PGSA samples from Batch number 2. Both figures showed low adherence, but the cell were alive after 24 hours.

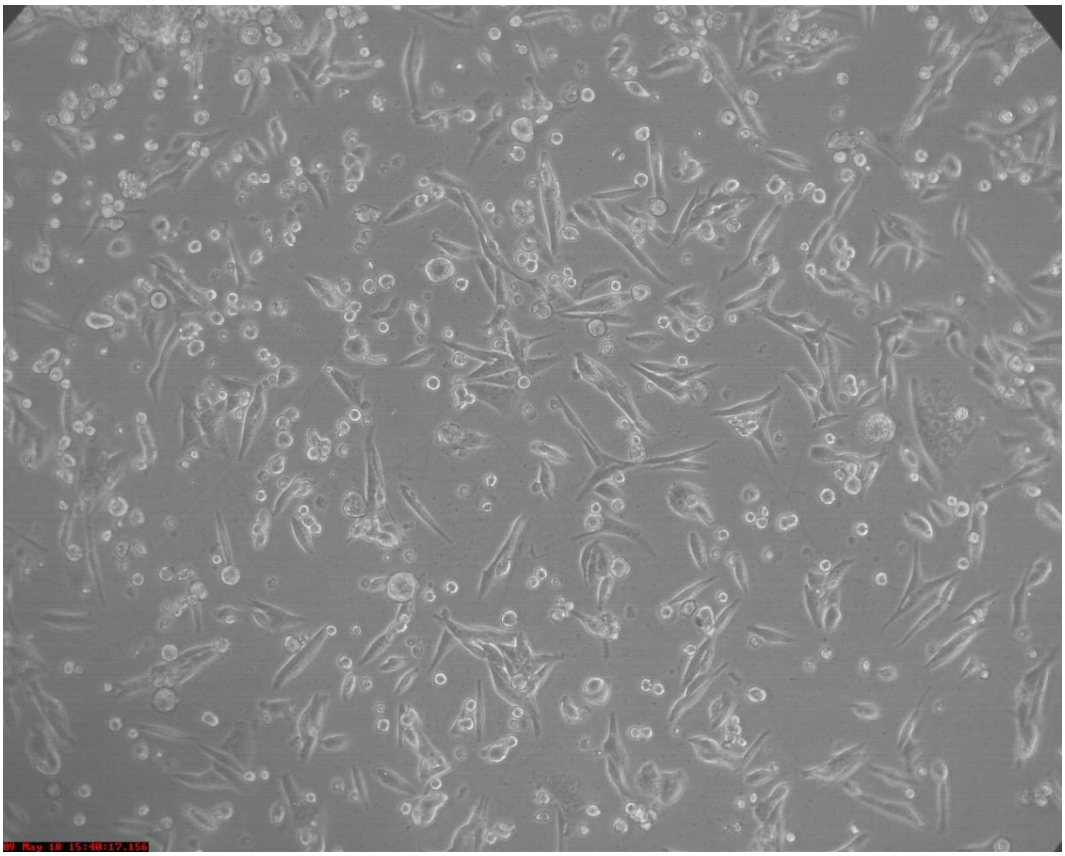

Figure 49. Cell on the bottom of the dish of the biocompatibility chambers from Batch 1

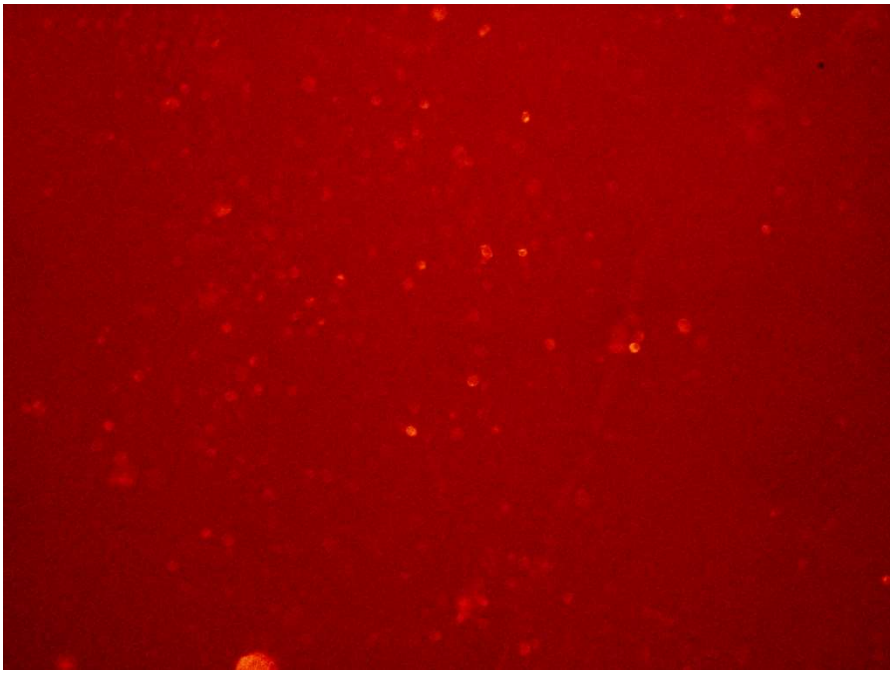

Figure 50. PGSA from Batch 1 compatibility results with tdTomato

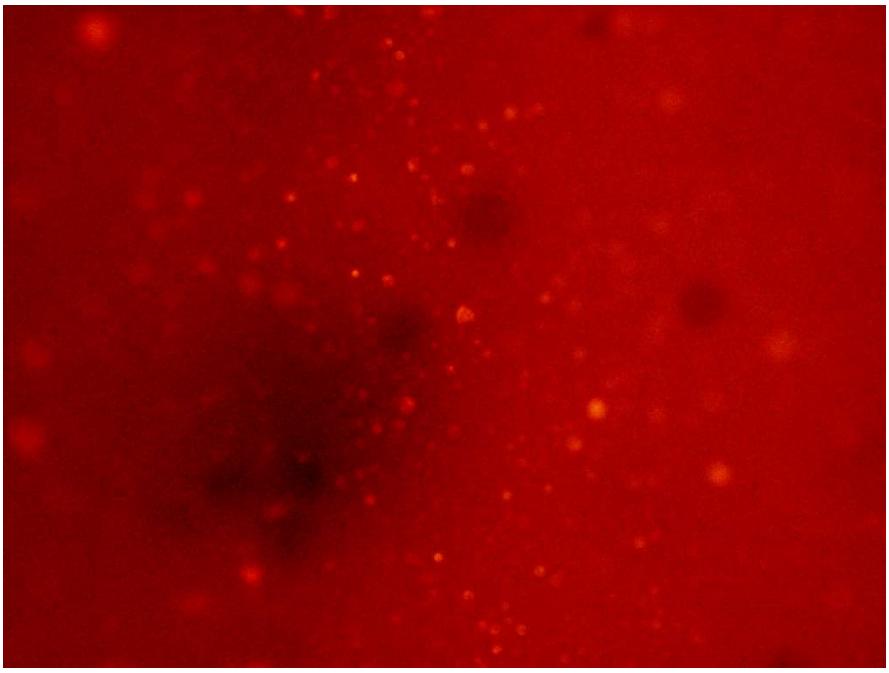

Figure 51. PGSA from Batch 2 compatibility results with tdTomato

The biocompatibility samples from Batch 3 showed the best results when compared to the other batches. A higher number of cells were visible on the polymer. However, due to the higher magnification (10X) images are distorted due to the depth of the chambers. Figure 52 and Figure 53 shows the corner of one of the biocompatibility samples. Cells are alive and have a mild adherence. Figure 54 shows how the cells agglomerated in the porosity of the polymer, which might be helpful for the proliferation of the cells in future scaffold designs.

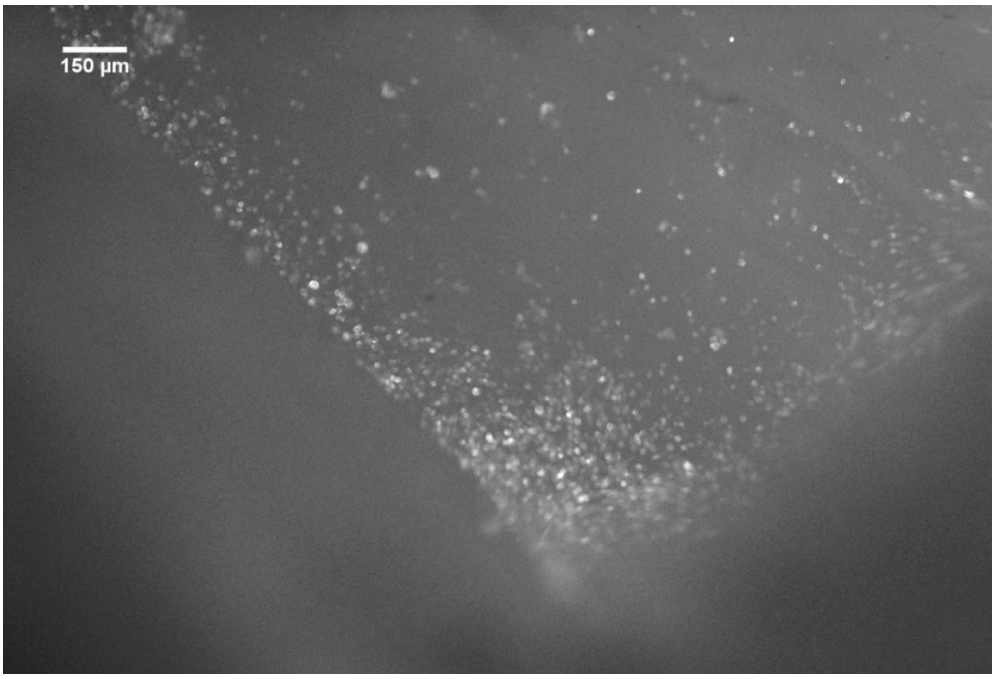

Figure 52. The corner of one of the biocompatibility samples from PGSA from Batch 3 showing better viability

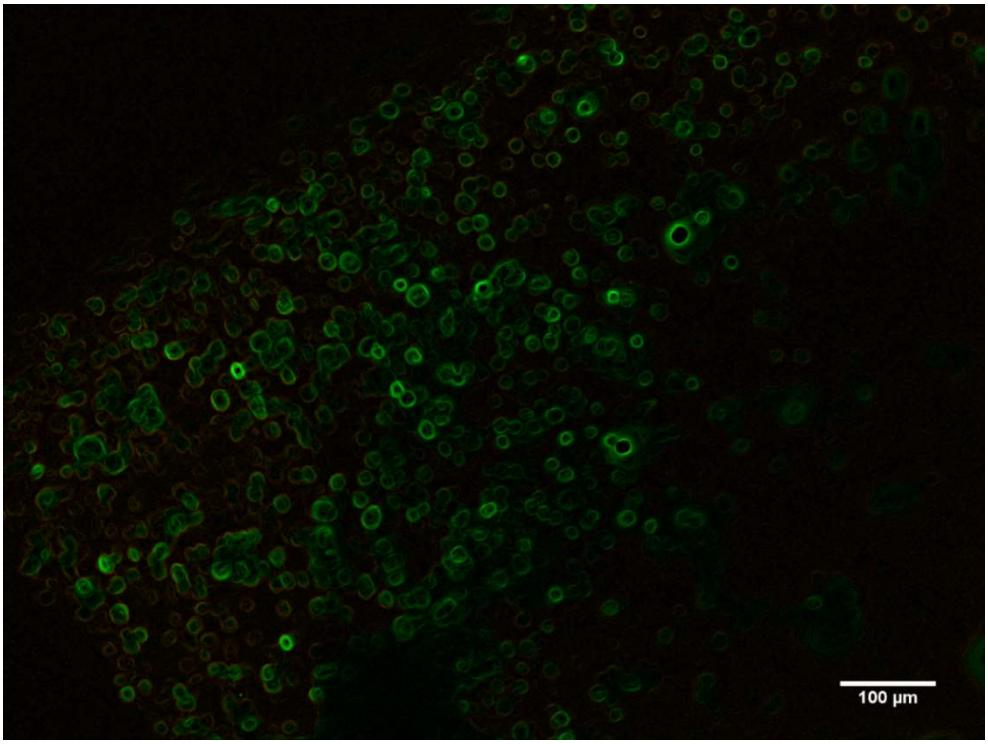

Figure 53. Biocompatibility chambers from Batch 3 highlighting the outer membrane of the cells

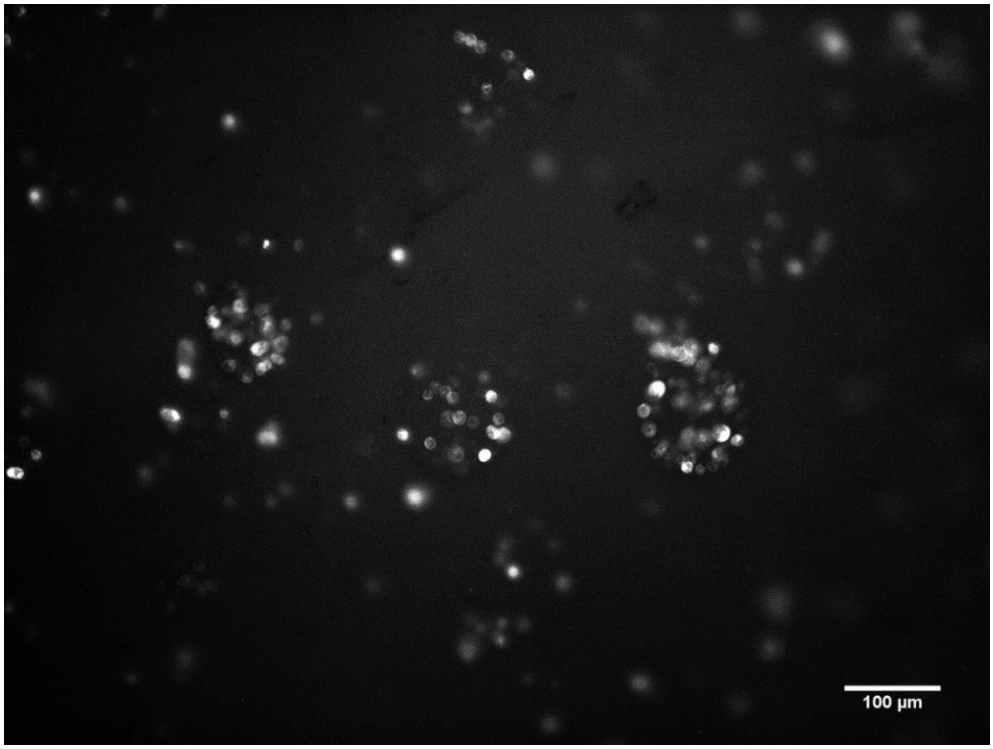

Figure 54. PGSA samples from Batch 3 with agglomerations of cells on porous

4.6 3D Printing Results

The main goal of the project of successfully LCD 3D print PGSA was completed. All the biocompatibility/swelling chambers and tensile samples were manufactured for the respective tests. As shown in Figure 55, on one of the first trials of 3D printing PGSA, the material successfully adhered to the print bed, and it is not damaged by the pealing forces on the material. For future goals, the development of more complex shapes should be explored like a bronchial tree scaffold for epithelial regeneration. The results of the biocompatibility chambers and the 3D printed tensile samples are shown in Figure 56 and Figure 57.

Figure 55. Primary tests of 3D printing PGSA proving that a thin layer of the material adheres to the building plate

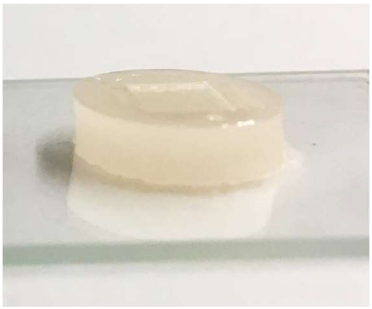

Figure 56. Side view of 3D printed biocompatibility chambers

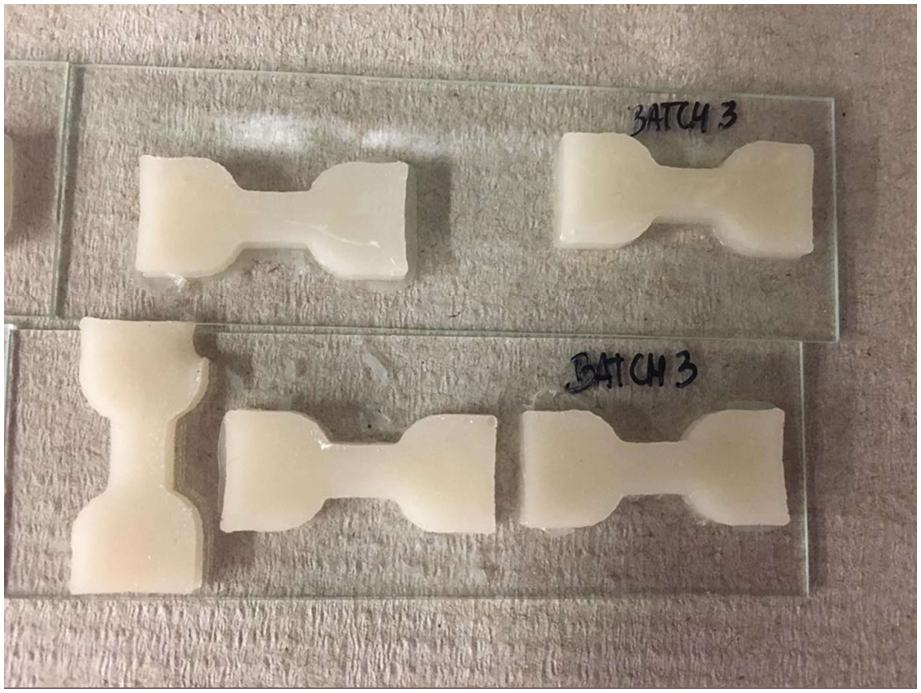

Figure 57. 3D printed tensile tests samples dry from Batch 3

5 SUMMARY AND CONCLUSION

The main goal of this thesis was to synthesize a version of PGSA biomaterial that can be 3D printed using an LCD 3D printer. This project demonstrates that LCD 3D printing is a viable option to create biodegradable and biocompatible scaffolds for biomedical applications using a photocurable elastomers. 3D printed objects can be created much faster than traditional methods with much higher accuracy and is less expensive than other bioprinting options.

The curing time of the PGS prepolymer was significantly decreased from approximately 72 hours to 3 to 4 hours as the reaction temperature was increased to 140°C and moisture produced in the reaction was removed periodically. The FTIR spectrum of the PGS prepolymer presented comparable signature bands with an intense stretch of the C=0 at 1696 cm^{-1} that confirms the formation of ester linkages and an intense OH stretch at 3500-3200 cm^{-1} indicating that the hydroxyl groups. The addition of acrylate groups was confirmed with the appearance of an absorption band that represents the CH stretching of the second alkyl group at 1375cm^{-1}. The formation of the polymer network after photocuring PGSA was confirmed by the increase of the 1731.4cm^{-1}, and reduction of the absorption bands of hydroxyl (3500-3200 cm^{-1}) with a significant reduction of the peak at 1375 cm^{-1}, known to be associated with acrylate groups. Therefore, these results were found to be similar from previously published papers, proving that these alterations on the synthesis process of the polymer did not have a significant effect on the material.

The average viscosity of PGSA was found to be 3.57±0.17 Pa.s for PGSA Batch 1, 3.62±0.16 Pa.s for PGSA Batch 2, and 15.62±0.90 Pa.s for PGSA Batch 3. For the

traditional 3D printed resins, it was found that the average viscosity of the FormLabs resin was 2.19±0.04 Pa.s and the average MakerJuice viscosity was found to be 0.12±0.01 Pa.s. Therefore, the average viscosity of PGSA was higher than other commonly used 3D printed resins, however, it is still inside the range of allowable 3D printed viscosities which is lower than 20 Pa.s.

The swelling results of the polymer indicated that the polymer is hydrophobic, and it does significantly swell, up to 13.11% for Batch 3, but after equilibrium is reached, its swelling ratio stayed more constant (decreased to 9.22% after 72 hours) for Batch 3 than form the other batches. For Batch 1 and 2, after 72 hours, the polymer had a significant drop of about 10% of the swelling ratio, which could cause damages in the polymer. The samples from Batch 1 presented a weight lower than its original weight, showing that degradation started earlier on that Batch.

The mechanical properties of 3D printed PGSA presented stiffer characteristics for Batch 3, with a Young's Modulus of Elasticity of 1.2750±0.464 MPa. This result was expected since the prepolymer had the higher molecular weight than the other two Batches. The polymer that had the least amount of curing time, from Batch 1, presented the characteristic elastomeric curve for the mechanical test, with a Young's Modulus of Elasticity of 0.0039±0 MPa. The samples from Batch 2 were between the batches 1 and 3, with a Young's Modulus of Elasticity of 0.3893±0.07MPa. Therefore, it can be concluded that the mechanical properties can be tailored by changes to the curing process of the material, such as decreasing pre-polymer curing time for a more elastomeric polymer or increasing the curing time for a more stiffer material.

The 3D printed biocompatibility chambers showed good cell viability with a high number of live cells on top of the biocompatibility chambers and mild amount of adherence (which can be improved by adding collagen). The cells that did not attach to the chamber were also alive in the bottom of the dish, proving that the polymer did not produce any toxic components to the cells. The results also showed how the cells agglomerated in the porous created in the material, which proves that the proliferation of the cells in future scaffold designs are possible. Therefore, since the cells were alive in the bottom of all the dishes and they adhered to the biocompatibility chamber, it can be concluded that the biomaterial is non-toxic and that the cells have the potential to adhere and proliferate in PGSA.

In conclusion, LCD 3D printing is simple, fast and can provide excellent resolution. The combination of LCD 3D printing and PGSA is a very promising tool for biomedical applications that allows complex biocompatible, elastomeric tissue scaffolds that can be highly customized without modifying the manufacturing process. Further 3D printing of complex scaffolds has the potential to successfully be used in multiple biomedical applications including epithelial regeneration.

6 FUTURE WORK

The system designed as part of this work has some areas that could be improved, as well as overall efficacy. Suggested improvements to the system include:

- Improvements to the LCD 3D Printer - Changes should be made to ease the manufacturing process of 3D printing, such as decreasing the size of the printing bed and vat according to the desired application. This will allow the user to fill the vat with a smaller batch of material and allow the printer to "load" more material in between layers. Currently, the vat is too large and material is manually loaded in between layers. Furthermore, changing the LCD screen to a more precise and accurate digital mask that does not absorb as much of the light intensity will significantly decrease the curing time of PGSA. Possible replacement options would be to use a projector as a light source with a DMD mask, however this would also require modifications to a light wavelength of 525nm.
- Additional biocompatibility studies - Further biocompatibility tests will be required to prove that PGSA is a reliable option for epithelial regeneration. If the keratinocytes survive in the material and form epithelial sheets, that is a significant scientific advance. Moreover, transepithelial electrical resistance (TEER) is a valid option for assessing proliferation of the epithelial cells. Additionally, biocompatibility test should be performed on 3D printed complex structures, to verify that the cell can successfully grow in a controlled matter in a scaffold with complex shapes (bronchial three). Also, scaffolds for different stratified squamous epithelial tissues replacements,

like skin, rectum, intestines or mucosa of the mouth or esophagus should be developed. Moreover, better methods of obtaining biocompatibility images should be explored, so the Eosin Y does not affect the end results with its fluorescence.

- Improvements to the polymer - PGSA is a difficult material to work with, because of its main advantage of being highly customized. The synthesis and manufacturing process must be as consistent as possible, in order to not create any unreliable batches/results. Additionally, keeping the temperature and pressure constant during the prepolymer reaction is of extreme importance. Furthermore, at least two more batches of the same prepolymer curing time should be developed to have more data points and improve the data analysis.
    - Moreover, not only the prepolymer curing time of the polymer can affect the mechanical properties of the PGSA samples, but also the curing time on the printer. In this study, the materials were over-cured in order to assess how the prepolymer curing time would affect the mechanical properties of the samples, but further studies should be performed to access how the printing curing time can affect the 3D printed samples of PGSA.

7 REFERENCES

[1] C.L. Ventola, Medical Applications for 3D Printing: Current and Projected Uses, P&T 39(10) (2014).

[2] R.J. Mondschein, A. Kanitkar, C.B. Williams, S.S. Verbridge, T.E. Long, Polymer structure-property requirements for stereolithographic 3D printing of soft tissue engineering scaffolds, Biomaterials 140 (2017) 170-188.

[3] N.A. Sears, D.R. Seshadri, P.S. Dhavalikar, E. Cosgriff-Hernandez, A Review of Three-Dimensional Printing in Tissue Engineering, Tissue Eng Part B Rev 22(4) (2016) 298-310.

[4] F.J. O'Brien, Biomaterials & scaffolds for tissue engineering, Materials Today, 2011.

[5] Nasim Annabi, Jason W. Nichol, Xia Zhong, Chengdong Ji, Sandeep Koshy, Ali Khademhosseini, Fariba Dehghani, Controlling the Porosity and Microarchitecture of Hydrogels for Tissue Engineering, Tissue Engineering Part B 16(4) (2010).

[6] Q.L. Loh, C. Choong, Three-dimensional scaffolds for tissue engineering applications: role of porosity and pore size, Tissue Eng Part B Rev 19(6) (2013) 485-502.

[7] X. Zhang, C. Jia, X. Qiao, T. Liu, K. Sun, Porous poly(glycerol sebacate) (PGS) elastomer scaffolds for skin tissue engineering, Polymer Testing 54 (2016) 118-125.

[8] K. WHANG, K.E. HEALY, D.R. ELENZ, E.K. NAM, D.C. TSAI, C.H. THOMAS, G.W. NUBER, F.H. GLORIEUX, R. TRAVERS, S.M. SPRAGUE, Engineering Bone Regeneration with Bioabsorbable Scaffolds with Novel Microarchitecture, Tissue Engineering 5(1) (1999).

[9] V. Karageorgiou, D. Kaplan, Porosity of 3D biomaterial scaffolds and osteogenesis, Biomaterials 26(27) (2005) 5474-91.

[10] S. Gerecht, S.A. Townsend, H. Pressler, H. Zhu, C.L. Nijst, J.P. Bruggeman, J.W. Nichol, R. Langer, A porous photocurable elastomer for cell encapsulation and culture, Biomaterials 28(32) (2007) 4826-35.

[11] S.J. Hollistera, R.D. Maddoxa, J.M. Taboasa, Optimal design and fabrication of scaffolds to mimic tissue properties and satisfy biological constraints, Biomaterials 23(20) (2002) 4095-4103.

[12] P. Zhang, Z. Hong, T. Yu, X. Chen, X. Jing, In vivo mineralization and osteogenesis of nanocomposite scaffold of poly(lactide-co-glycolide) and hydroxyapatite surface-grafted with poly(L-lactide), Biomaterials 30(1) (2009) 58-70.

[13] C. Ji, N. Annabi, A. Khademhosseini, F. Dehghani, Fabrication of porous chitosan scaffolds for soft tissue engineering using dense gas CO2, Acta Biomater 7(4) (2011) 1653-64.

[14] J. Hu, D. Kai, H. Ye, L. Tian, X. Ding, S. Ramakrishna, X.J. Loh, Electrospinning of poly(glycerol sebacate)-based nanofibers for nerve tissue engineering, Mater Sci Eng C Mater Biol Appl 70(Pt 2) (2017) 1089-1094.

[15] P. Bajaj, R.M. Schweller, A. Khademhosseini, J.L. West, R. Bashir, 3D biofabrication strategies for tissue engineering and regenerative medicine, Annu Rev Biomed Eng 16 (2014) 247-76.

[16] E. Bakaic, N.M.B. Smeets, T. Hoare, Injectable hydrogels based on poly(ethylene glycol) and derivatives as functional biomaterials, RSC Adv. 5(45) (2015) 35469-35486.

[17] L. Ouyang, C.B. Highley, C.B. Rodell, W. Sun, J.A. Burdick, 3D Printing of Shear-Thinning Hyaluronic Acid Hydrogels with Secondary Cross-Linking, ACS Biomaterials Science & Engineering 2(10) (2016) 1743-1751.

[18] J. Zhu, P. He, L. Lin, D.R. Jones, R.E. Marchant, Biomimetic poly(ethylene glycol)-based hydrogels as scaffolds for inducing endothelial adhesion and capillary-like network formation, Biomacromolecules 13(3) (2012) 706-13.

[19] W. Shi, R. He, Y. Liu, 3D printing scaffolds with hydrogel materials for biomedical applications, European Journal of BioMedical Research 1(3) (2015).

[20] Y. He, W.-b. Wu, J.-z. Fu, Rapid fabrication of paper-based microfluidic analytical devices with desktop stereolithography 3D printer, RSC Advances 5(4) (2015) 2694-2701.

[21] C. Zhou, Y. Chen, Z. Yang, B. Khoshnevis, Digital material fabrication using mask-image-projectionbased stereolithography, Rapid Prototyping J 19(153) (2013).

[22] X. Garric, O. Guillaume, H. Dabboue, M. Vert, J.P. Moles, Potential of a PLA-PEO-PLA-based scaffold for skin tissue engineering: in vitro evaluation, J Biomater Sci Polym Ed 23(13) (2012) 1687-700.

[23] C.G. Jeong, S.J. Hollister, A comparison of the influence of material on in vitro cartilage tissue engineering with PCL, PGS, and POC 3D scaffold architecture seeded with chondrocytes, Biomaterials 31(15) (2010) 4304-12.

[24] E. Ye, P.L. Chee, A. Prasad, X. Fang, C. Owh, V.J.J. Yeo, X.J. Loh, Supramolecular soft biomaterials for biomedical applications, Materials Today 17(4) (2014) 194-202.

[25] W.S. Toh, X.J. Loh, Advances in hydrogel delivery systems for tissue regeneration, Mater Sci Eng C Mater Biol Appl 45 (2014) 690-7.

[26] Y. Wang, G. Ameer, B. Sheppard, R. Langer, A tough biodegradable elastomer, Nature Biotechnology 20(6) (2002) 602-6.

[27] K.W. Lee, Y. Wang, Elastomeric PGS scaffolds in arterial tissue engineering, J Vis Exp (50) (2011).

[28] C.A. Sundback, J.Y. Shyu, Y. Wang, W.C. Faquin, R.S. Langer, J.P. Vacanti, T.A. Hadlock, Biocompatibility analysis of poly(glycerol sebacate) as a nerve guide material, Biomaterials 26(27) (2005) 5454-64.

[29] C.D. Pritchard, K.M. Arner, R.S. Langer, F.K. Ghosh, Retinal transplantation using surface modified poly(glycerol-co-sebacic acid) membranes, Biomaterials 31(31) (2010) 7978-84.

[30] J.M. Kemppainen, S.J. Hollister, Tailoring the mechanical properties of 3D-designed poly(glycerol sebacate) scaffolds for cartilage applications, J Biomed Mater Res A 94(1) (2010) 9-18.

[31] Z.J. Sun, C. Chen, M.Z. Sun, C.H. Ai, X.L. Lu, Y.F. Zheng, B.F. Yang, D.L. Dong, The application of poly (glycerol-sebacate) as biodegradable drug carrier, Biomaterials 30(28) (2009) 5209-14.

[32] R. Rai, M. Tallawi, A. Grigore, A.R. Boccaccini, Synthesis, properties and biomedical applications of poly(glycerol sebacate) (PGS): A review, Progress in Polymer Science 37(8) (2012) 1051-1078.

[33] C.L. Nijst, J.P. Bruggeman, J.M. Karp, L. Ferreira, A. Zumbuehl, C.J. Bettinger, R. Langer, Synthesis and characterization of photocurable elastomers from poly(glycerol-co-sebacate), Biomacromolecules 8(10) (2007) 3067-73.

[34] Y. Wang, Y.M. Kim, R. Langer, In vivo degradation characteristics of poly(glycerol sebacate), Biomedical Materials Research (66A) (2003) 192-197.

[35] C.G. Williams, A.N. Malik, T.K. Kim, P.N. Manson, J.H. Elisseeff, Variable cytocompatibility of six cell lines with photoinitiators used for polymerizing hydrogels and cell encapsulation, Biomaterials 26(11) (2005) 1211-8.

[36] B.D. Fairbanks, M.P. Schwartz, C.N. Bowman, K.S. Anseth, Photoinitiated polymerization of PEG-diacrylate with lithium phenyl-2,4,6-trimethylbenzoylphosphinate: polymerization rate and cytocompatibility, Biomaterials 30(35) (2009) 6702-7.

[37] A.D. Rouillard, C.M. Berglund, J.Y. Lee, W.J. Polacheck, Y. Tsui, L.J. Bonassar, B.J. Kirby, Methods for photocrosslinking alginate hydrogel scaffolds with high cell viability, Tissue Eng Part C Methods 17(2) (2011) 173-9.

[38] Z. Wang, R. Abdulla, B. Parker, R. Samanipour, S. Ghosh, K. Kim, A simple and high-resolution stereolithography-based 3D bioprinting system using visible light crosslinkable bioinks, Biofabrication 7(4) (2015) 045009.

[39] V. Srivastava, P.P. Singh, Eosin Y catalysed photoredox synthesis: a review, RSC Advances 7(50) (2017) 31377-31392.

[40] H. Shih, C.C. Lin, Visible-light-mediated thiol-ene hydrogelation using eosin-Y as the only photoinitiator, Macromol Rapid Commun 34(3) (2013) 269-73.

[41] M. Bacakova, J. Musilkova, T. Riedel, D. Stranska, E. Brynda, L. Bacakova, M. Zaloudkova, The potential applications of fibrin-coated electrospun polylactide nanofibers in skin tissue engineering, International Journal of Nanomedicine (2016).

[42] P. Zanger, Staphylococcus aureus positive skin infections and international travel, Wien Klin Wochenschr 122 Suppl 1 (2010) 31-3.

[43] M. Matsusaki, K. Fujimoto, Y. Shirakata, S. Hirakawa, K. Hashimoto, M. Akashi, Development of full-thickness human skin equivalents with blood and lymph-like capillary networks by cell coating technology, J Biomed Mater Res A 103(10) (2015) 3386-96.

[44] H.Y. Lin, H.H. Chen, S.H. Chang, T.S. Ni, Pectin-chitosan-PVA nanofibrous scaffold made by electrospinning and its potential use as a skin tissue scaffold, J Biomater Sci Polym Ed 24(4) (2013) 470-84.

[45] D. Singh, D. Singh, S. Han, 3D Printing of Scaffold for Cells Delivery: Advances in Skin Tissue Engineering, Polymers 8(1) (2016).

[46] G.J. Tortora, M.T. Nielsen, Principles of Human Anatomy Kaye Pace, Wiley, 2014.

[47] D.N. Coakley, F.M. Shaikh, K. O'Sullivan, E.G. Kavanagh, P.A. Grace, T.M. McGloughlin, In vitro evaluation of acellular porcine urinary bladder extracellular matrix – A potential scaffold in tissue engineered skin, Wound Medicine 10-11 (2015) 9-16.

[48] K. Vig, A. Chaudhari, S. Tripathi, S. Dixit, R. Sahu, S. Pillai, V.A. Dennis, S.R. Singh, Advances in Skin Regeneration Using Tissue Engineering, Int J Mol Sci 18(4) (2017).

[49] L.J. Pourchet, A. Thepot, M. Albouy, E.J. Courtial, A. Boher, L.J. Blum, C.A. Marquette, Human Skin 3D Bioprinting Using Scaffold-Free Approach, Adv Healthc Mater 6(4) (2017).

[50] J. Venkatesan, R. Jayakumar, S. Anil, E.P. Chalisserry, R. Pallela, S.-K. Kim, Development of Alginate-Chitosan-Collagen Based Hydrogels for Tissue Engineering, Journal of Biomaterials and Tissue Engineering 5(6) (2015) 458-464.

[51] H.Y. Lin, S.H. Chen, S.H. Chang, S.T. Huang, Tri-layered chitosan scaffold as a potential skin substitute, J Biomater Sci Polym Ed 26(13) (2015) 855-67.

[52] T.W. Wang, J.S. Sun, H.C. Wu, Y.H. Tsuang, W.H. Wang, F.H. Lin, The effect of gelatin-chondroitin sulfate-hyaluronic acid skin substitute on wound healing in SCID mice, Biomaterials 27(33) (2006) 5689-97.

[53] E.J. Chong, T.T. Phan, I.J. Lim, Y.Z. Zhang, B.H. Bay, S. Ramakrishna, C.T. Lim, Evaluation of electrospun PCL/gelatin nanofibrous scaffold for wound healing and layered dermal reconstitution, Acta Biomater 3(3) (2007) 321-30.

[54] M.S. Taylor, A.U. Daniels, K.P. Andriano, J. Hellert, Six Bioabsorbable Polymers: In Vitro Acute Toxicity of Accumulated Degradation Products, Journal of Applied Biomaterials Vol. 5(15) (1994) 1 - I57.

[55] B. Derby, Printing and Prototyping of Tissues and Scaffolds, Science 338(6109) (2012) 921-926.

[56] W.L. Ng, S. Wang, W.Y. Yeong, M.W. Naing, Skin Bioprinting: Impending Reality or Fantasy?, Trends Biotechnol 34(9) (2016) 689-699.

[57] W. Lee, J.C. Debasitis, V.K. Lee, J.H. Lee, K. Fischer, K. Edminster, J.K. Park, S.S. Yoo, Multi-layered culture of human skin fibroblasts and keratinocytes through three-dimensional freeform fabrication, Biomaterials 30(8) (2009) 1587-95.

[58] V. Lee, G. Singh, J.P. Trasatti, C. Bjornsson, X. Xu, T.N. Tran, S.S. Yoo, G. Dai, P. Karande, Design and fabrication of human skin by three-dimensional bioprinting, Tissue Eng Part C Methods 20(6) (2014) 473-84.

[59] L. Koch, A. Deiwick, S. Schlie, S. Michael, M. Gruene, V. Coger, D. Zychlinski, A. Schambach, K. Reimers, P.M. Vogt, B. Chichkov, Skin tissue generation by laser cell printing, Biotechnol Bioeng 109(7) (2012) 1855-63.

[60] S. Michael, H. Sorg, C.T. Peck, L. Koch, A. Deiwick, B. Chichkov, P.M. Vogt, K. Reimers, Tissue engineered skin substitutes created by laser-assisted bioprinting form skin-like structures in the dorsal skin fold chamber in mice, PLoS One 8(3) (2013) e57741.

[61] N. Cubo, M. Garcia, J.F. Del Canizo, D. Velasco, J.L. Jorcano, 3D bioprinting of functional human skin: production and in vivo analysis, Biofabrication 9(1) (2016) 015006.

[62] C.J. Bettinger, B. Orrick, A. Misra, R. Langer, J.T. Borenstein, Microfabrication of poly (glycerol-sebacate) for contact guidance applications, Biomaterials 27(12) (2006) 2558-65.

[63] M. Radisic, H. Park, T.P. Martens, J.E. Salazar-Lazaro, W. Geng, Y. Wang, R. Langer, L.E. Freed, G. Vunjak-Novakovic, Pre-treatment of synthetic elastomeric scaffolds by cardiac fibroblasts improves engineered heart tissue, J Biomed Mater Res A 86(3) (2008) 713-24.

[64] W.L. Neeley, S. Redenti, H. Klassen, S. Tao, T. Desai, M.J. Young, R. Langer, A Microfabricated Scaffold for Retinal Progenitor Cell Grafting, Biomaterials 29(4) (2008) 418–426.

[65] A. Mahdavi, L. Ferreira, C. Sundback, J.W. Nichol, E.P. Chan, D.J.D. Carter, C.J. Bettinger, S. Patanavanich, L. Chignozha, E. Ben-Joseph, A. Galakatos, H. Pryor, I. Pomerantseva, P.T. Masiakos, A. Zumbueh, S. Hong, J. Borenstein, J. Vacanti, R. Langer, J.M. Karp, A biodegradable and biocompatible gecko-inspired tissue adhesive, PNAS 105(7) (2008) 2307–2312.

[66] J.L. Ifkovits, R.F. Padera, J.A. Burdick, Biodegradable and radically polymerized elastomers with enhanced processing capabilities, Biomed Mater 3(3) (2008) 034104.

[67] J.L. Ifkovits, J.J. Devlin, G. Eng, T.P. Martens, G. Vunjak-Novakovic, J.A. Burdick, Biodegradable fibrous scaffolds with tunable properties formed from photo-cross-linkable poly(glycerol sebacate), ACS Appl Mater Interfaces 1(9) (2009) 1878-86.

[68] Y.C. Yeh, C.B. Highley, L. Ouyang, J.A. Burdick, 3D printing of photocurable poly(glycerol sebacate) elastomers, Biofabrication 8(4) (2016) 045004.

[69] Y.-C. Yeh, L. Ouyang, C.B. Highley, J.A. Burdick, Norbornene-modified poly(glycerol sebacate) as a photocurable and biodegradable elastomer, Polym. Chem. 8(34) (2017) 5091-5099.

[70] R. Maliger, P.J. Halley, J.J. Cooper-White, Poly(glycerol-sebacate) bioelastomers-kinetics of step-growth reactions using Fourier Transform (FT)-Raman spectroscopy, Journal of Applied Polymer Science 127(5) (2013) 3980-3986.

[71] R. Rai, M. Tallawi, N. Barbani, C. Frati, D. Madeddu, S. Cavalli, G. Graiani, F. Quaini, J.A. Roether, D.W. Schubert, E. Rosellini, A.R. Boccaccini, Biomimetic poly(glycerol sebacate) (PGS) membranes for cardiac patch application, Mater Sci Eng C Mater Biol Appl 33(7) (2013) 3677-87.

[72] I.H. Jaafar, M.M. Ammar, S.S. Jedlicka, R.A. Pearson, J.P. Coulter, Spectroscopic evaluation, thermal, and thermomechanical characterization of poly(glycerol-sebacate) with variations in curing temperatures and durations, Journal of Materials Science 45(9) (2010) 2525-2529.

[73] E.M. Jeffries, R.A. Allen, J. Gao, M. Pesce, Y. Wang, Highly elastic and suturable electrospun poly(glycerol sebacate) fibrous scaffolds, Acta Biomater 18 (2015) 30-9.

[74] X.J. Loh, A. Abdul Karim, C. Owh, Poly(glycerol sebacate) biomaterial: synthesis and biomedical applications, J. Mater. Chem. B 3(39) (2015) 7641-7652.

[75] A. Tevlek, H.M. Aydin, Poly(Glycerol-Sebacate) Elastomer A Mini Review, Ortho Surg Open Access (OSOA.000507) (2017) 1(2).

[76] Q.Z. Chen, H. Ishii, G.A. Thouas, A.R. Lyon, J.S. Wright, J.J. Blaker, W. Chrzanowski, A.R. Boccaccini, N.N. Ali, J.C. Knowles, S.E. Harding, An elastomeric patch derived from poly(glycerol sebacate) for delivery of embryonic stem cells to the heart, Biomaterials 31(14) (2010) 3885-93.

[77] A. Tevlek, P. Hosseinian, C. Ogutcu, M. Turk, H.M. Aydin, Bi-layered constructs of poly(glycerol-sebacate)-beta-tricalcium phosphate for bone-soft tissue interface applications, Mater Sci Eng C Mater Biol Appl 72 (2017) 316-324.

[78] S.H. Zaky, K.W. Lee, J. Gao, A. Jensen, K. Verdelis, Y. Wang, A.J. Almarza, C. Sfeir, Poly (glycerol sebacate) elastomer supports bone regeneration by its

mechanical properties being closer to osteoid tissue rather than to mature bone, Acta Biomater 54 (2017) 95-106.

[79] S.H. Zaky, K.W. Lee, J. Gao, A. Jensen, J. Close, Y. Wang, A.J. Almarza, C. Sfeir, Poly(glycerol sebacate) elastomer: a novel material for mechanically loaded bone regeneration, Tissue Eng Part A 20(1-2) (2014) 45-53.

[80] V. Mourino, A.R. Boccaccini, Bone tissue engineering therapeutics: controlled drug delivery in three-dimensional scaffolds, J R Soc Interface 7(43) (2010) 209-27.

[81] I.S. Tobias, H. Lee, G.C. Engelmayr, Jr., D. Macaya, C.J. Bettinger, M.J. Cima, Zero-order controlled release of ciprofloxacin-HCl from a reservoir-based, bioresorbable and elastomeric device, J Control Release 146(3) (2010) 356-62.

[82] P.M. Lambert, C.B. Williams, T.E. Long, L.R. Bickford, Design and Fabrication of a Mask Projection Microstereolithography System for the Characterization and Processing of Novel Photopolymer Resins, Mechanical Engineering, Virginia Polytechnic Institute and State University 2014.

[83] Y. Pan, C. Zhou, Y. Chen, A Fast Mask Projection Stereolithography Process for Fabricating Digital Models in Minutes, Journal of Manufacturing Science and Engineering 134(5) (2012).

[84] C. Sun, N. Fang, D.M. Wu, X. Zhang, Projection micro-stereolithography using digital micro-mirror dynamic mask, Sensors and Actuators A: Physical 121(1) (2005) 113-120.

[85] X. Zheng, J. Deotte, M.P. Alonso, G.R. Farquar, T.H. Weisgraber, S. Gemberling, H. Lee, N. Fang, C.M. Spadaccini, Design and optimization of a light-emitting diode

projection micro-stereolithography three-dimensional manufacturing system, Rev Sci Instrum 83(12) (2012) 125001.

[86] M. Farsari, F. Claret-Tournier, S. Huang, C.R. Chatwin, D.M. Budgett, P.M. Birch, R.C.D. Young, J.D. Richardson, A novel high-accuracy microstereolithography method employing an adaptive electro-optic mask, Journal of Materials Processing Technology 107 (2000) 167±172.

[87] A. Bertsch, S. Zissi, J.Y. Je´ze´quel, J.C.A. S. Corbel, Microstereophotolithography using a liquid crystal display as dynamic mask-generator, Microsystem Technologies (1997) 42—47.

[88] K. Pal, A.K. Banthia, D.K. Majumdar, Polymeric Hydrogels: Characterization and Biomedical Applications, Designed Monomers & Polymers 12(3) (2009) 197-220.

[89] J.J. Harris, B. Nicholson, C. Smoot, Rheology of poly(glycerol sebacate) Poster, Society of Biomaterials, 2014.

[90] MakerJuice SF Data Sheet 2014. https://cdn.shopify.com/s/files/1/1224/0904/files/SFMSDS.pdf?17439595932289550931. 2018).

[91] Formlabs photopolymer resin Grey, 2015. https://formlabs.com/media/upload/Grey-SDS_lQLbyNE.pdf. 2018).

[92] Examples of Rheology Testing Techniques, 2013. http://www.rheologyschool.com/testing/testing-examples. (Accessed November 30th, 2017).